AUDITORY PERCEPTION AND CORTICAL PLASTICITY AFTER LONG-TERM BLINDNESS

Elizabeth Huber

A dissertation

submitted in partial fulfillment of the

requirements for the degree of

Doctor of Philosophy

University of Washington

2016

Reading Committee:

Ione Fine, Chair

Geoffrey M. Boynton

Scott O. Murray

Adrian K.C. Lee

Program Authorized to Offer Degree:

Psychology

University of Washington

Abstract

Auditory perception and cortical plasticity after long-term blindness

Elizabeth Huber

Chair of the Supervisory Committee:
Professor Ione Fine
Department of Psychology

The study of blindness provides a context for examining neural plasticity in the adult and developing brain, and for asking basic questions about the principles that guide neural computation in sensory cortex. By noting how a system operates when its inputs are altered, we gain insight into the rules that govern its function. The experiments described in this dissertation combine functional magnetic resonance imaging (fMRI) with behavioral methods and computational modeling to examine three issues: (1) Does longstanding blindness affect the cortical representation of auditory frequency? (2) Can we relate cortical representations of auditory frequency to behavioral discrimination, and/or to higher-order phenomena like auditory motion processing? (3) How do visual and auditory responses in adult sight-recovery subjects compare to responses observed in individuals without a history of blindness, and in those with sustained blindness?

TABLE OF CONTENTS

LIST OF FIGURES

LIST OF TABLES

OVERVIEW

In blindness, the visual brain stays active, seemingly engaged in a host of non-visual sensory and cognitive functions. Much recent work has aimed to uncover the rules that govern this reorganization. For instance, a currently influential framework suggests that cortex can be characterized in terms of "functional constancies", or a "meta-modal" organization (Pascual-Leone & Hamilton, 2001; Pascual-Leone et al., 2005), in which brain areas serve fixed computational roles, regardless of input modality. In this context, researchers have sought analogies between cross-modal responses due to blindness and the functional modularity observed in non-deprived cortex. While this framework has proved useful in many cases (e.g., Mahon, 2009; Buchel et al., 1998; Reich et al., 2011; Collignon et al., 2011; Renier et al., 2010; Saenz et al., 2008; Jiang et al., 2014), it fails to predict, for example, responses related to language in primary visual cortex (Bedny et al., 2011).

Moreover, while it is generally supposed that compensatory plasticity within occipital cortex should underlie supra-normal behavioral performance in blind humans, only a handful of studies have successfully linked such performance with neural measures (Renier et al., 2013; Voss et al., 2011; Stevens et al., 2007; Gougoux et al., 2005; Amedi et al., 2005, 2003; Cohen et al., 1997). Even fewer links have been made with measures in non-deprived sensory areas (Sterr et al., 1998; Roder et al., 1999). As further complication, the literature contains conflicting reports on the presence of behavioral enhancements among blind individuals, due in part to the small sample sizes routinely used in these experiments (Kupers et al., 2014). For instance, while a number of behavioral studies link early-onset blindness to superior pitch perception (Gougoux et al.,

2004; Wan et al., 2010; Voss and Zatorre, 2012), others have shown equivalent performance in blind and sighted subjects (Collignon et al., 2013; Watkins et al., 2013; Starlinger & Niemeyer, 1981). It would therefore be premature to make strong claims about either the prevalence or magnitude of these putative effects.

This dissertation describes a series of experiments examining cortical representations of auditory frequency following early and sustained blindness, and sight-recovery during adulthood (Chapter 1-2), alongside an investigation of visual processing following more than a decade of recovered sight (Chapter 3). Where possible, we seek to link behavioral performance with neural measures, using computational models of BOLD fMRI.

The first section examines the effects of early blindness on auditory frequency discrimination and frequency tuning within auditory cortex. Using fMRI and an adaptation of the population receptive field technique (Dumoulin and Wandell, 2008; Thomas et al., 2015), we measured voxel-wise frequency tuning within auditory cortex, in both blind and sighted individuals. In the same group of subjects, we then measured frequency discrimination thresholds, to test for differences in performance as a result of blindness. Finally, we used a linking model to relate neural responses and behavioral performance, showing that relative responses across frequency within primary auditory cortex correlated strongly with behavioral frequency discrimination.

The second section of this dissertation describes an fMRI experiment investigating auditory selectivity within early 'visual' areas in four early-blind individuals, and in two individuals who regained sight during adulthood after long-term blindness. In these subjects, we observed novel representations of auditory frequency

within cortical visual motion area hMT+, which lends credence to the notion that hMT+ might serve analogous computational roles in the visually deprived and non-deprived brain, as discussed in Chapter 2.

Further, frequency selectivity in hMT+ was observed not only in early-blind individuals, but also in two sight-recovery subjects, including one who had normal visual development up to age three. While the co-localization of auditory and visual motion responses is intriguing, it should be noted that our analysis of the BOLD response cannot be used to infer that the same neural circuits underlie visual and auditory motion processing in these individuals: The relevant neural populations may simply overlap at the relatively coarse spatial scale of fMRI. Future work employing, for example, fMRI adaptation methods, should lend further insight into the extent of cross-modal allocation of neural resources in these individuals.

In the final section of this dissertation, I present the results of a follow-up study examining visual perception and cortical responses in one of the sight recovery subjects described in Chapter 2. Despite showing robust responses to visual motion in hMT+, this individual had highly attenuated category-selective activity in ventral visual cortex, alongside severe behavioral impairments in 3-D form, object, and face processing, even after more than a decade of recovered vision. These data complement an existing literature, which emphasizes that restoring optical input is not the same as restoring useful vision (Cheselden, 1727; Gregory & Wallace, 1963; Valvo, 1971; Fine et al., 2003; Sinha & Held, 2012; Šikl et al., 2013). Our data highlight the consequences of deprivation starting at late as age 3, even after extensive visual experience in adulthood.

CHAPTER 1. Early blindness shapes cortical representations of auditory frequency

In collaboration with Jessica M. Thomas, Geoffrey M. Boynton, and Ione Fine

Early onset blindness has been linked to superior auditory abilities, which may be mediated by compensatory plasticity within auditory and/or occipital cortex. Here we examine the effects of early blindness on the cortical representation of auditory frequency and behavioral frequency discrimination using fMRI and psychophysics. Within primary auditory cortex, we observe narrower tuning bandwidths in a group of early blind individuals, providing some of the first evidence the blindness leads to systematic changes in neural tuning within a non-deprived sensory area. Early blind individuals did not show enhanced behavioral performance in our frequency discrimination task. However, a simple model linking cortical responses to behavioral performance successfully predicted performance as a function of frequency, and also predicted the lack of a behavioral difference between blind and sighted subjects.

INTRODUCTION

It has long been held that early blindness leads to enhanced pitch perception. Indeed, since the early 1800's, musical vocations - in particular, piano tuning - have been associated with blind individuals: In an 1884 census, 25% percent of employed blind individuals were musicians, including many piano tuners (Progress. Mar/Apr 1884, RNIB Archive). However, while a number of behavioral studies have linked early-onset blindness to superior pitch perception (Gougoux et al., 2004; Wan et al., 2010; Voss and

Zatorre, 2012), this finding has not always been replicated (Collignon et al., 2013; Watkins et al., 2013). Thus, neither the prevalence nor the magnitude of these effects can be stated with certainty.

Nor is the neural basis of these putative enhancements clear. It is possible that heightened frequency discrimination in early blind individuals might be mediated by compensatory plasticity within deprived occipital cortex. Responses to a variety of auditory stimuli have been found throughout occipital cortex, but clear evidence for frequency tuning has not been reported. Kujala and colleagues (1992) observed that responses to pure tones, measured using EEG, were shifted posteriorly in a group of blind subjects, and subsequent MEG measurements further suggested these responses might be localized to occipital cortex (Kujala et al., 1995). More recently, Watkins and colleagues (2013) used fMRI to show that voxels in visual motion area hMT+ varied in their frequency preferences in a subset of congenitally blind (anophthalmic) subjects. However, the presence of auditory frequency tuning within hMT+ did not predict behavioral performance on a pitch-change task, and it was not clear that the observed preferences reflected genuine tuning to auditory frequency.

Enhanced pitch perception in early blind individuals might also be mediated by changes within auditory areas. Previous MEG results suggested an expanded tonotopic representation within primary auditory cortex (Elbert et al., 2002), with responses to 500 and 4kHz tones being separated more widely on the cortical surface in blind relative to sighted individuals. An expanded tonotopic map might permit a finer frequency resolution and/or a larger overall representation of specific auditory frequencies, the latter having been linked to superior discrimination performance in adult owl monkeys

(Rencanzone et al., 1993). Finally, a number of studies have reported an *attenuated* response to auditory stimuli in the temporal lobe of early blind individuals (Gougoux et al., 2009; Stevens and Weaver, 2009; Watkins et al., 2013). This has variously been interpreted as reduced participation in auditory processing, perhaps due to function being usurped by reorganized occipital cortex (as occurs for auditory motion processing e.g., Jiang et al., 2014), or as increased 'efficiency' of processing within the intact modality.

Here, we characterize the effects of blindness on the cortical representation of auditory frequency. Using fMRI and an adaptation of the population receptive field technique (Dumoulin and Wandell, 2008; Thomas et al., 2015), we measured voxel-wise frequency tuning within canonical auditory sensory areas and occipital cortex, in both blind and sighted individuals. In the same group of subjects, we then measured frequency discrimination thresholds to test for differences in performance as a result of blindness. Finally, we use a linking model to relate neural responses with behavioral performance, showing that cortical representations of frequency can be used to predict behavioral thresholds.

METHODS

Participants

Four early blind (ages 32-55, 2 males; clinical descriptions given in Table 1) and four age-matched sighted subjects participated in one session of MR imaging and one session of psychophysical testing. Subjects reported normal hearing and no history of neurological or psychiatric illness. All procedures, including recruitment, consent, and testing, followed the guidelines of the University of Washington Human Subjects Division and were reviewed and approved by the UW Institutional Review Board.

Subject	Sex	Age	Clinical description
EB01	Male	32	Leber's congenital amaurosis, low light perception
EB02	Female	38	Retinopathy of prematurity, no light perception in right eye, minimal peripheral light perception in left eye, 3 months premature
EB03	Female	55	Retinopathy of prematurity, low light perception until retina detached at age 25, 2 months premature
EB04	Male	52	Congenital glaucoma, no light perception

Table 1.1. Subject demographics and clinical descriptions.

Auditory stimulus creation

Auditory stimuli were generated in MATLAB using the Psychophysics Toolbox (www.psychtoolbox.org) and custom software and delivered via insert earphones. MR compatible Sensimetrics S86 earphones were used within the scanner. Etymotic ER2 earphones were used for psychophysics outside the scanner. All stimuli were presented at

a sampling rate of 44.1 kHz, with intensities adjusted to ensure flat frequency transmission from 100 Hz to 8 kHz. Subjects were instructed to keep their eyes closed throughout testing, and overhead lighting was switched off during MRI acquisition.

Magnetic resonance imaging

Acquisition protocol

Functional magnetic resonance images were acquired with a 3T Phillips Achieva scanner (Philips, Eindhoven, Netherlands) at the University of Washington Diagnostic Imaging Sciences Center (DISC) using a 32-channel head coil. Foam padding was used to minimize head motion.

In each session, four functional scans were acquired using a standard EPI sequence (36 slices, TR/TE = 2000/25ms, flip angle = 80°, no slice gap). After discarding the first 5 timeframes, each scan consisted of 255 volumes at an effective voxel size of 3.00 mm isotropic.

Auditory stimulus and task

After system calibration, stimulus sound intensities were adjusted according to a standard equal-loudness curve created for insert earphones (ISO 226) to equate perceived loudness across frequency. Actual sound intensities (65–83 dB SPL) were matched to the perceived loudness of a 1 kHz tone (reference frequency) at 70 dB SPL. Acoustic noise from the scanner was attenuated by expanding-foam ear-tips, as well as protective earmuffs placed over the ear following earphone insertion. Subjects confirmed that all tones were clearly audible, and of roughly equal loudness across the frequency range.

Stimuli were blocks of pure tone bursts, which varied in auditory frequency (88-8000 Hz, sampled in half octave steps). Briefly, each 2 s stimulus block contained eight pure tone bursts of the same frequency, presented in a rhythmic pattern to facilitate perceptual segregation of the stimulus from background scanner noise (see Da Costa et al., 2011; Thomas et al, 2015). Each run consisted of a series of sequences of 3-4 ascending or descending half-octave steps, with the starting frequency and sequence (ascending vs. descending) selected pseudo randomly at the beginning of each sequence. The pseudo randomization ensured that the distribution of presented frequencies between 88-8000Hz was uniform, and that there were equal numbers of ascending and descending sequences.

Subjects were asked to monitor stimulus frequency and perform a 1-back task in which they responded via button press each time a stimulus block repeated the exact frequency of the previous tone burst (10% of trials).

MR data pre-processing

For analysis, functional data were resampled into $1 \times 1 \times 1$ mm^3 volumetric space. Standard pre-processing of fMRI data was carried out using BrainVoyager QX software (version 2.3.1 Brain Innovation B.V., Maastricht, The Netherlands), including 3D motion correction and high-pass filtering (cut-off: 3 cycles). Parameters generated during motion correction were recorded to ensure that (1) subject motion within a scan did not exceed 3mm or 3 degrees of rotation, and (2) blind and sighted subjects did not show differential motion within scans.

Functional data were aligned to the T1-weighted anatomical image acquired in the same session (MPRAGE, $1 \times 1 \times 1$ mm^3). The BrainVoyager QX automatic segmentation routine was used to reconstruct the cortical surface at the white–gray matter border (with hand-editing to minimize segmentation errors) and the resulting smooth 3D surface was partially inflated.

Anatomical voxel selection

For each subject, large anatomical regions of interest (ROIs) were selected from the partially inflated left and right hemisphere cortical surface meshes using drawing tools in BrainVoyager QX. The *auditory cortex* ROI consisted of all voxels within a contiguous region between the lateral border on the crown of the superior temporal gyrus, the medial border within the fundus of the lateral sulcus, the posterior border of the supramarginal gyrus, and the anterior border of the most anterior portion of the temporal lobe. The *occipital cortex* ROI was selected to run from the parietal-occipital fissure to the occipital pole.

All surface-defined ROIs were then mapped back into the brain volume and expanded to include voxels from -1 to 3 mm around the gray-white matter boundary. Preprocessed time-course data for each 3D anatomical voxel within the volume ROIs were then exported to Matlab for further analysis.

Population receptive field analysis for frequency mapping

Preprocessed fMRI data within the anatomical ROIs were analyzed using methods described in detail in Thomas et al. (2015). In brief, we assumed that each voxel within

an anatomically defined region of interest had a one dimensional Gaussian sensitivity profile on a log auditory frequency axis. Predicted time-series were created by convolving a binary matrix marking the presence or absence of auditory stimulation over frequency and time with a model of the hemodynamic response (HRF, see below) and a the hypothetical Gaussian pRF, whose center (f_0) and standard deviation (σ) were free to vary. Using custom software written in MATLAB, we found, for each voxel, the center (f_0) and standard deviation (σ) of the Gaussian that when multiplied by the stimulus over time and convolved with a hemodynamic response function produced a predicted time course that best correlated with the voxel's measured time course. For each voxel, the best-fitting value of f_0 is interpreted as that voxel's preferred frequency, while the best-fitting value of σ is used to calculate the Gaussian full width at half max, which is interpreted as that the tuning bandwidth.

We modeled the auditory HRF as a gamma function, with the initial parameters n=3, tau (τ)=1.5, and delay (δ)=2.25, based on Boynton et al. (1996). To obtain individual HRF estimates, we optimized τ and δ for each subject while holding f_0 and σ fixed. This estimate was only carried out on a subset of the data (1 out of 4 scans) with a fitted correlation value above 0.25 and within the anatomically defined ROIs, to limit computational time and avoid over-fitting the data. Median τ and δ parameters were used to estimate each individual's HDR. We then iteratively fit the pRF parameters (f_0 and σ) for all voxels within the ROI, using the individually fitted HRF parameters. Individual HRF parameters are reported in Table 1.2. For early blind subjects, parameters estimates within auditory and occipital cortex are presented. All analyses were replicated using data

fitted with the initial HRF parameters (n=3, τ=1.5, δ=2.25), which produced slightly reduced goodness-of-fit values but did not change any of the findings described here.

Subject	**Tau, delay (auditory / occipital)**
EB01	0.4414, 3.6906 / 0.2483, 2.4478
EB02	1.0108, 1.7264 / 1.1827, 1.8680
EB03	1.1019, 3.4896 / 1.4267, 4.7648
EB04	1.3869, 2.8454 / 1.9014, 1.9465
SC01	0.2729, 3.8117
SC02	0.2937, 3.6873
SC03	1.0904, 2.8147
SC04	1.6669, 1.1831

Table 1.2. Individually fitted HDR parameters for auditory and occipital cortex in early blind individuals, and auditory cortex in sighted individuals.

After fitting, only voxels that met the following criteria were retained for further analyses: (1) the correlation between the observed fMRI time-course and the time-course predicted by the best-fitting pRF (our goodness-of-fit index) was higher than 0.20, (2) the center (f_0) of the best fitting pRF fell within the range of tested values (88-8000 Hz), and (3) the standard deviation (σ) of the best fitting pRF fell between 0.075 (half the minimum inter-tone-interval) and 2 (the full presented frequency range) in log frequency. We additionally estimated a response scaling factor, a, that minimized the mean squared error between the measured time-course for each voxel and a predicted time-course. Thus, voxels that passed these criteria could be described in terms of three parameters: the center (f_0), standard deviation (σ), and amplitude (a) of the best fitting Gaussian.

PAC ROI

For simplicity, we refer here to the pair of tonotopic gradients comprising hA1 and hR as "primary auditory cortex" (PAC). In primates, the auditory "core" area contains up to three tonotopic subdivisions, A1, R, and RT (Hackett et al., 1998; Hackett, 2008), which have been localized to the medial two-thirds of Heshl's gyrus (Rademacher et al., 2001; Dick et al., 2012). Human neuroimaging studies have identified at least two tonotopic gradients, presumed to be the human homologues of areas A1 and R (Formisano et al., 2003; Humphries et al., 2010; Da Costa et al., 2011; Langers and van Dijk, 2011; Striem-Amit et al., 2011; Moerel et al., 2012; Da Costa et al., 2011; Da Costa et al., 2013; Thomas et al., 2015)

Here, we similarly identified two mirror-symmetric tonotopic gradients, meeting at a low-frequency reversal on the crown of Heshl's gyrus. Based on this tonopic map and the underlying anatomy, a PAC ROI was defined as a contiguous patch of cortical surface spanning Heschl's gyrus and containing both tonotopic gradients. Anterior and posterior borders were drawn along the outer high-frequency representations of the tonotopic maps, and lateral and medial borders were conservatively drawn to include only the medial two-thirds of Heschl's gyrus.

Psychophysics

Stimulus and task

Each participant completed one detection experiment (two blocks of 300 trials) and one discrimination experiment (four blocks of 300 trials) in a single session lasting approximately 2 hours, with rest breaks given as needed.

For both the detection and discrimination experiments, stimuli consisted of six tones spanning the frequency range used in the fMRI session: 200, 400, 800, 1600, 3200, and 6400 Hz. A linear amplitude ramp was applied to remove acoustic artifacts at stimulus onset and offset. Psychophysical tests were carried out in a sound-attenuated room, and subjects wore protective earmuffs to further dampen residual acoustic noise.

Detection experiment

The detection experiment was used to estimate each subject's audiogram, to confirm subjects' self-reported normal hearing and rule-out group differences in sensitivity at the frequencies of interest. An interleaved staircase procedure was used to present each of the 6 frequencies. The stimulus frequency presented on each trial was chosen pseudo-randomly, and subjects reported which of two temporal intervals contained the tone (versus silence). Independent 3-up 1-down staircases were used to estimate each subject's detection threshold for each frequency.

Discrimination experiment

The discrimination experiment was used to estimate the just-noticeable-difference (JND, the difference in frequency producing 80% correct performance) for each of the six standard tones listed above. Peak stimulus amplitude was matched to that used in the fMRI experiment. On each trial, subjects heard pairs of tones, each lasting 300ms with a 0s inter-stimulus-interval, and were asked to judge whether the second tone was higher or lower in frequency than the first (2-alternative forced choice). Once again, an interleaved staircase procedure was used to present each of the 6 frequencies. The stimulus frequency

presented on each trial was chosen pseudo-randomly, and independent 3-up 1-down staircases were used to estimate each subject's JND for each frequency.

Statistical Analyses

Given the relatively small sample (n=4) size used here, we cannot be assured that our data meet the assumptions of parametric tests, and therefore we have opted for a non-parametric approach. Statistical significance of group comparisons was estimated using the Wilcoxon rank sum test, a non-parametric test of the equality of population medians based on sample data (Wilcoxon, 1945), which serves as a distribution-free alternative to the two-sample t-test.

Comparisons of frequency distributions across groups were performed using a bootstrapped $\chi 2$ test of independence. The traditional $\chi 2$ test compares obtained frequency distributions across each group with the expected outcome were distributions independent of group assignment, with a large $\chi 2$ value suggesting that group membership influences frequency distributions (McHugh, 2013). The significance of the $\chi 2$ value was estimated using a bootstrapping procedure implemented with custom software, which simply re-estimated $\chi 2$ after randomly assigning subjects to either group (10,000 simulations) to find the probability of randomized $\chi 2$ values exceeding the obtained $\chi 2$. Subjects (rather than voxels or hemispheres) were randomly assigned between groups.

RESULTS

Tonotopic mapping in auditory cortex

Across groups, we report no statistically significant difference in the size of PAC, as defined by the total number of voxels with a pRF model fit of $R>0.2$ (Wilcoxon rank sum test: $p=0.0571$), or in the total surface area of PAC (Wilcoxon rank sum test: $p=0.4857$).

Figures 1.1 and 1.2 show best-frequency and tuning bandwidths on the auditory cortical surface. Tonotopic maps within auditory cortex are visually similar across blind and sighted subject groups, and no group dependence was observed in a statistical comparison of the early blind and sighted best-frequency distributions ($\chi 2(3,13)=100.8213$, $p<0.4079$).

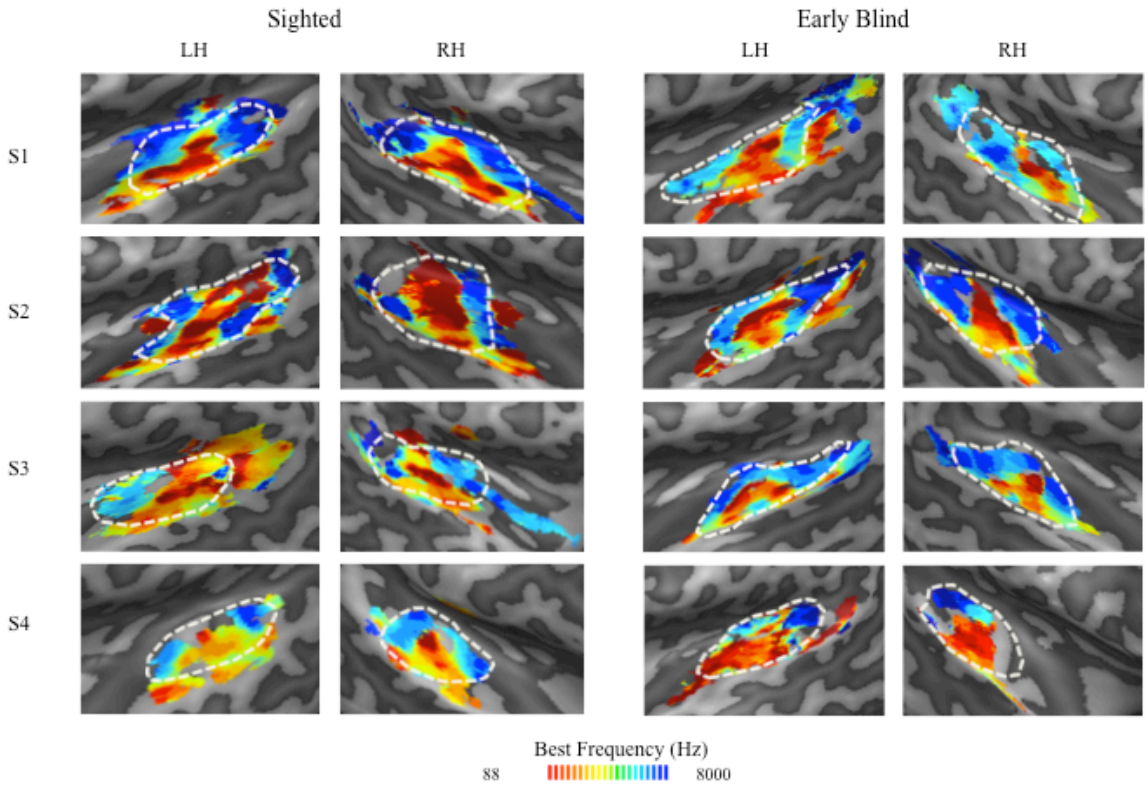

Figure 1.1. Tonotopic maps for the left and right hemispheres of sighted and early blind subjects. Frequency center (f_0) values are color-coded along a gradient, with red corresponding to the lowest frequency value (88 Hz) through blue corresponding to the highest frequency (8000 Hz). The borders of the PAC ROIs are designated by dashed white lines. The crowns of gyri are indicated by the dashed black lines. Maps are thresholded at R>0.2, except for early-blind S4, who was thresholded at R > 0.1 in Figures 1 and 2 solely for visualization purposes.

Figure 1.2 shows tuning bandwidths on the cortical surface. The warmer colors within PAC reflect the narrower tuning bandwidths in blind compared to sighted subjects (Wilcoxon rank sum test: p=0.0379). Figure 2.3B quantifies this effect, and further shows that these reduced tuning widths were seen within the lower and middle frequency range.

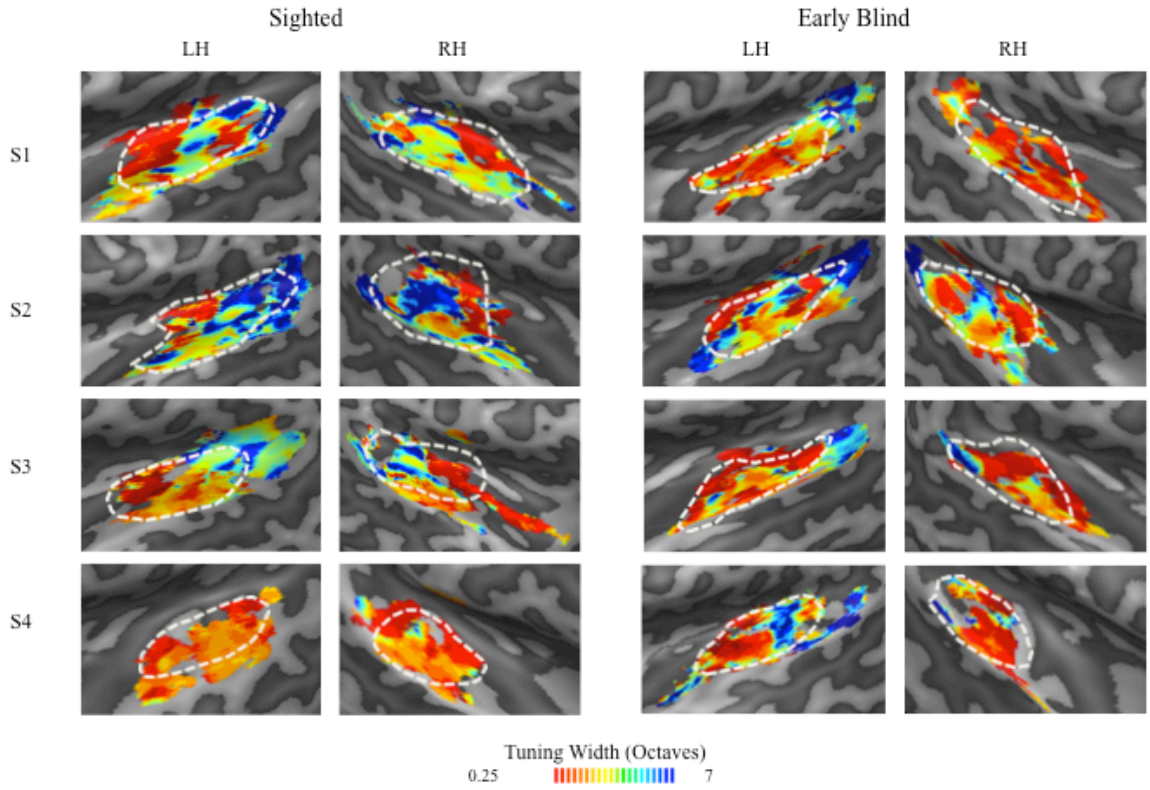

Figure 1.2. Tuning bandwidth maps for the left and right hemispheres of sighted and early blind subjects. Tuning width (σ) values are color-coded along a gradient, with red corresponding to the narrowest bandwidths (.25 octaves) through blue corresponding to the largest bandwidths (7 octaves). Maps are thresholded at R>0.2, except for early-blind S4, who was thresholded at R > 0.1 in Figures 1 and 2 solely for visualization purposes.

Figure 1.3A summarizes the best frequency distributions within PAC as the proportion of all voxels assigned to each frequency. Voxels were sorted into half-octave bins based on their best-frequency values (f_0). The reduced representation of middle (~700-1400 Hz) frequencies likely reflects, in part, the effects of acoustic scanner noise, as shown in Figure 1.3C. Although the location of pRF best-frequency estimates should not be strongly biased by acoustic scanner noise (Thomas et al., 2015), acoustic masking

might degrade the fits for pRFs centered on frequencies heavily represented in the scanner noise, resulting in fewer voxels passing threshold.

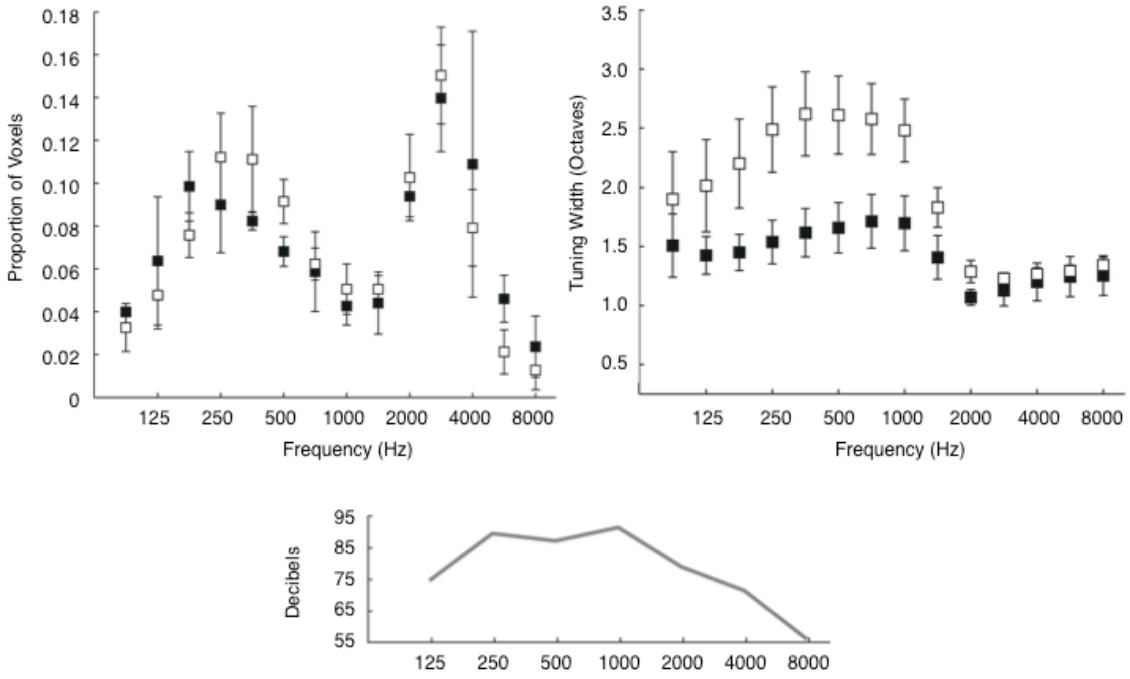

Figure 1.3. PRF center counts, tuning width, and scanner noise plotted as a function of frequency. (A) Voxel proportions, sorted into half-octave bins based on pRF best-frequencies (f_0) for early blind (black symbols) and sighted (white symbols) subjects. (B) PRF tuning width as a function of frequency. Voxels were sorted into the same half-octave bins, and mean tuning width was calculated for each bin. Symbols represent group means with single standard errors calculated across subjects. Tuning widths differed between blind and sighted groups, most notably across the lower and middle frequency range. (C) Acoustic scanner noise level, in dB, as a function of frequency.

Amplitude

As described in the Introduction, a number of studies report an *attenuated* response to sound in the temporal lobe of blind individuals (Gougoux et al., 2009; Stevens and Weaver, 2009; Watkins et al., 2013). Interestingly, as shown in Figure 1.4, when a using a conventional GLM analysis of sound vs. silence (collapsing across frequency) in PAC, we replicated these findings of weaker BOLD responses in early

blind subjects, although we detect no difference in pRF amplitudes fitted using our model (Wilcoxon rank sum test: p=0.3429). As described in the Discussion, tuning bandwidths were previously shown to correlate with BOLD response magnitudes in a different group of sighted subjects (Thomas et al, 2015). We suggest that the narrower tuning bandwidths in early blind subjects similarly provide the misleading appearance of a reduced BOLD response when voxel tuning functions are not explicitly modeled.

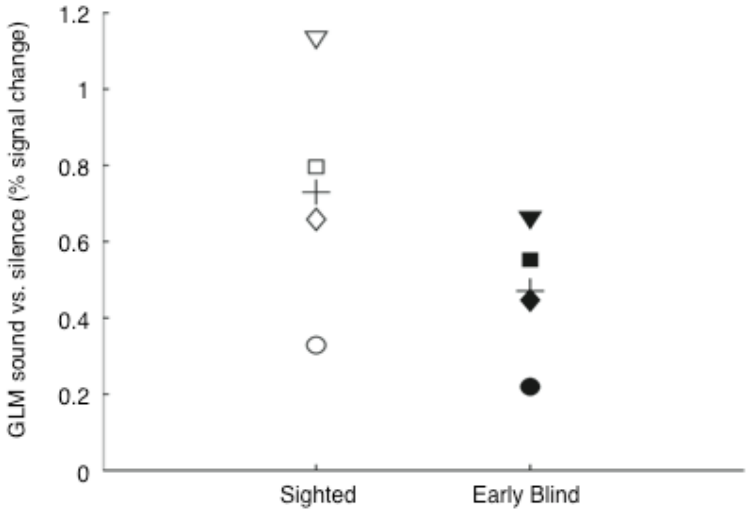

Figure 1.4. Response amplitudes within PAC estimated using a GLM analysis of sound vs. silence for blind (black symbols) and sighted (white) subjects. Group means are indicated by crossed-lines. Like past studies, we find that auditory cortex shows an overall reduced response to sound in the blind group. However, we find no difference across groups in pRF amplitudes, and we attribute the reduced response to difference in tuning width as described in the main text.

Frequency tuning in occipital cortex

Within occipital cortex we find evidence for tuning to auditory frequency in two early blind individuals, and none of the sighted controls. These data are described in

greater detail in CHAPTER 2 of this dissertation. Where present, occipital tuning favored mid-range frequencies, and had similar bandwidths to those found within early blind PAC.

Auditory frequency discrimination

Figure 1.5A shows thresholds as a function of frequency for blind and sighted subjects. We find no evidence for superior discrimination performance among early blind individuals (Wilcoxon rank sum test: p=0.5887).

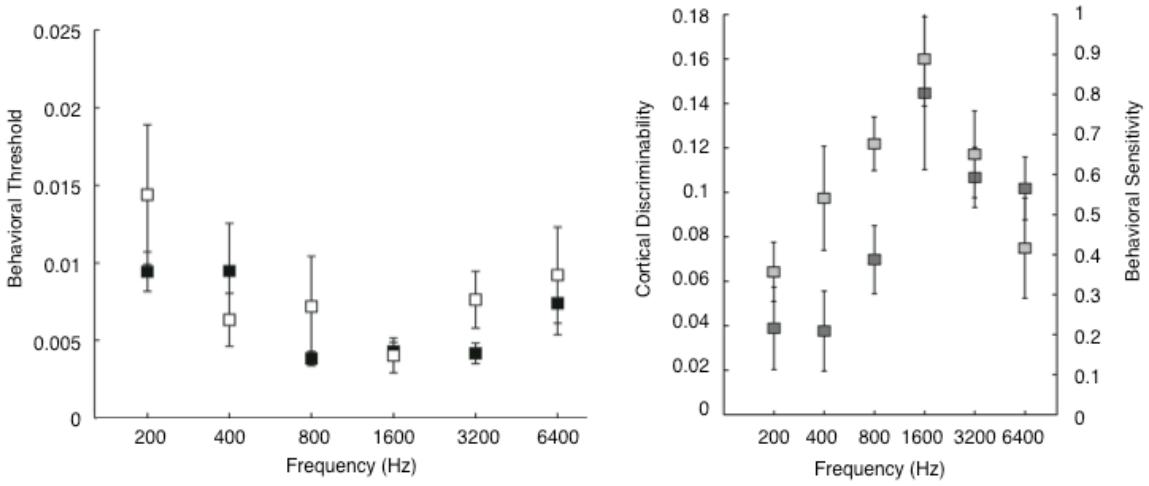

Figure 1.5. Behavioral thresholds and cortical discriminability. (A) Thresholds as a function of frequency for early blind (black symbols) and sighted (white symbols) subjects. The x-axis is the frequency, in Hz, of each standard tone, and the y-axis represents the increase in frequency (as a proportion of the standard tone frequency) producing 80% correct performance. (B) Normalized behavioral sensitivity (light gray) and normalized cortical discriminability (dark gray), averaged across blind and sighted subjects.

Modeling psychophysical performance using pRFs

The narrower tuning bandwidths observed in blind subjects did not correspond to superior discrimination performance in these individuals. However, the pRF model permits us to test whether differences in performance as a function of frequency might be predicted by the *cortical representation* of frequency. We therefore examined whether we could predict behavioral performance on the basis of *cortical discriminability* – defined as the change in cortical response across voxels elicited by two different stimuli.

For each subject, the best-fitting pRFs were used to create a vector representing the predicted response of every voxel (v) to any given frequency. This generated a vector (R_1) representing the predicted response to each of the 6 standard tones used in the behavioral experiment, and a corresponding vector (R_2) representing the response to each tone plus a fixed increment in (log) frequency. We modeled the discriminability between each tone pair (standard and incremented) as the sum of squared differences between these cortical response vectors. This produces a cortical discriminability index, *c,* for each subject and pair of frequencies:

$$c = \sqrt{\sum_{v=1}^{n} (R_{1v} - R_{2v})^2}$$

Cortical discriminability as a function of frequency is plotted in Figure 1.5B for all subjects (dark gray). Consistent with our results for behavioral performance, estimates of cortical discriminability did not differ across subject groups (Wilcoxon rank test: p=0.9372). Normalized behavioral sensitivity (1/threshold), averaged across blind and

sighted subjects, is plotted alongside cortical discriminability in 1.5B (light gray). Cortical discriminability closely matches behavioral sensitivity as a function of frequency (Spearman correlation carried out on ranks: $r=0.7143$, $p<0.05$). Within the early blind group, the correlation between cortical discriminability and behavioral sensitivity was slightly reduced when occipital voxels were included in the cortical discriminability metric for the two early blind subjects showing occipital tuning to frequency.

DISCUSSION

We report that early blindness changes the cortical representation of auditory frequency, resulting in narrower tuning bandwidths within PAC in a group of early blind individuals. Our data provide some of the first evidence for systematic changes in neural tuning within human PAC as a result of blindness. In contrast to previous studies with early blind individuals, we failed to observe enhanced behavioral performance in a frequency discrimination task. However, a simple model linking cortical responses to behavioral performance successfully predicted performance as a function of frequency, and also predicted the lack of a behavioral difference between blind and sighted subjects.

Cross-modal recruitment of occipital cortex

Within occipital cortex, we found voxels tuned for auditory frequency within two of our early blind subjects. Voxel tuning favored for mid-range frequencies, with similar bandwidths to those found within early blind PAC. Given that our paradigm elicited robust tonotopic maps within auditory cortex, it is unlikely that our analysis merely failed to detect analogous representations within occipital cortex. However, it is possible that our stimulus and task were suboptimal for driving responses in occipital cortex. Previous studies suggest that occipital cortex responds to a wide range of auditory stimuli (Lewis & Fine, 2011; for a recent review, see Kupers & Ptito, 2014), so it is possible that the frequency selectivity we observe here is incidental to higher-level functions, such as segregation of acoustic objects, analysis of speech, or spatial localization. This idea is explored in greater depth in Chapter 2.

Effects of blindness on frequency representations within primary auditory cortex

Surprisingly few studies have examined the effects of sensory deprivation on non-deprived cortex. Blindness in combination with Braille proficiency has been shown to alter finger representations within primary somatosensory cortex in blind human subjects (Pascual-Leone and Torres, 1993), and visual deprivation in combination with increased whisking-frequency has been shown to expand somatosensory whisker representations in binocularly enucleated mice (Rauschecker, 1995; Goel et al., 2006). Studies examining the effects of visual deprivation on auditory cortex in animal models have suggested similar enhancements (see Lee and Whitt, 2015, for a recent review), as discussed below.

PAC size

We failed to find evidence for the expanded tonotopic representation suggested previously by Elbert and colleagues (2002). Given our small number of subjects, this result should be treated with caution. However, given our finding of reduced tuning bandwidths in early blind subjects, we argue that past studies suggesting an expanded tonotopic area should also be read cautiously. For instance, the apparent increase in source separation of high and low frequencies that they found in early blind subjects by Elbert and colleagues (2002) may have been driven by differences in tuning bandwidth. Broader bandwidths in sighted subjects would be expected to result in a correspondingly larger cortical area of activation for any given auditory frequency. This might, in turn, have reduced the apparent source separation of high and low frequencies (Golubic et al., 2011). Karlen and Krubitzer (2009) report a modest increase in the relative size of primary somatosensory cortex in binocularly enucleated opposums, and it remains

possible that primary auditory cortex undergoes a similar expansion in blind humans. However, to date, no clear evidence for an expansion of PAC in early blind subjects has been shown.

Tuning bandwidth

Here, we show that blind individuals had significantly narrower tuning for auditory frequency within PAC. Although these data are compatible with narrower neural tuning, as described below, it is important to recall that pRF size estimates are affected by multiple factors beyond individual neural receptive field size. These factors include systematic changes in preferred frequency across the cortical surface (i.e., the frequency gradient across the cortical surface), non-systematic variance in preferred frequency (jitter in frequency preference at a given location), and non-neural factors such as hemodynamic blur (Dumoulin and Wandell, 2008). We saw no difference in frequency gradients across the cortical surface or measured hemodynamic response between our subject groups. Thus it is likely that our results either reflect a narrowing in tuning bandwidth of individual neurons or a reduction in non-systematic variance in preferred frequency. Consistent with the notion that these differences might reflect genuine differences in neural tuning, Petrus et al. (2014) has recently found that dark exposure sharpens the frequency tuning of individual neurons within A1 in the mouse, which they related to increased neural discrimination.

Response amplitudes

We found no evidence for reduced response to sound in early blind PAC, based on our amplitude parameter, *a*, which scales the predicted BOLD response generated as the forward solution to our pRF model. Nor did we see any indication of a difference in the number of voxels that passed threshold using our pRF analysis across blind and sighted individuals.

However, with the same data, we found reduced responses in our early blind subjects using a GLM approach that compared sound to silence. The difference between these two measures suggests that previous findings of reduced responses in PAC using a pure tones vs. silence (Stevens and Weaver, 2009; Watkins et al., 2013) may result from narrower tuning, which would be expected to result in a smaller of region of cortex responding to any given narrowband stimulus, thereby reducing measured activation to sound, on average, across a region of interest. Thus, without an explicit model of voxel tuning functions, narrower tuning bandwidths in early blind subjects produce an inaccurate appearance of a reduced BOLD response. Indeed, Thomas et al. (2015) previously reported a positive correlation between GLM activation (t-statistic) to sound vs. silence and tuning bandwidths within the auditory cortex of sighted subjects – broader tuning bandwidths were associated with larger activation values.

Caveats

We limited our subject pool to early blind individuals with no hearing loss who were experienced in the scanner, and as a result this study relies on a small number of

subjects. We attempted to limit across group variance by choosing control subjects that were carefully matched for age, education level, handedness, auditory detection thresholds, and musical background.

Given our small sample size, our failure to find differences between the groups for either BOLD population receptive field response amplitudes or the overall size of the PAC should not be taken as strong evidence that such differences do not exist. However, our results do suggest a plausible alternative explanation for previous studies showing reduced responsiveness (Stevens and Weaver, 2009; Watkins et al., 2013) or an expanded representation (Elbert et al., 2002) within PAC that merits further examination.

Auditory frequency discrimination

While some previous studies (Gougoux et al., 2004; Wan et al., 2010; Voss and Zatorre, 2012), found differences in behavioral frequency discrimination between blind and sighted individuals, other studies, including ours, have failed to find clear differences (Starlinger and Niemeyer, 1981; Collignon et al., 2013; Watkins et al., 2013). A number of plausible explanations exist for this discrepancy among studies. First, there may be heterogeneity of skill within the blind population, with enhanced performance being limited to a subgroup of blind individuals (Lessard et al., 1998; Voss et al., 2011; Voss et al., 2015). Moreover, given that untrained frequency discrimination thresholds are subject to relatively high individual variation (Amitay et al., 2005) and studies on the effects of blindness (including the present one) frequently rely on relatively small sample sizes, it is possible that individual variation in performance among one or both groups might produce a pattern of misleading results in the literature.

Our finding of narrower frequency tuning within PAC suggests that blind subjects might demonstrate behavioral enhancements under conditions where narrower tuning would be expected to play a greater role, for example narrowband stimuli presented against a broadband noise background. Similarly, if narrower bandwidths mediate enhanced performance, it is possible that relatively subtle differences in experimental setup, such as the degree of unintended acoustic interference (e.g., from stimuli presented in free field vs. insert ear phones, different levels of environmental noise shielding, headphone distortion artifacts), might profoundly influence results. Ironically, our experimental conditions (high quality in-ear headphones, high noise shielding) may have served to minimize the advantages of narrow tuning.

Thus, although our finding of narrower tuning bandwidth does not seem to correspond to enhanced performance on a simple discrimination task, it may be possible in the future to relate narrower tuning widths within auditory cortex to enhanced performance on more environmentally realistic or complex tasks (e.g. speech in noise) in early blind individuals.

Linking pRFs and behavior

Finally, we used a linking model to relate stimulus discriminability with behavioral performance as a function of frequency. Cortical discriminability was highest for frequencies with low behavioral discrimination thresholds, and discriminability correlated with behavioral sensitivity across the range of frequencies tested. Further, our model of cortical discriminability failed to predict a group difference in performance, as narrower pRF bandwidths in early blind subjects did not produce improved

discriminability across different frequencies: With narrow tuning, two similar frequencies produce relatively large differences in cortical responses within a relatively small number of voxels. With broader tuning, response differences tend to be smaller but are spread across a larger number of voxels. Therefore, in our model, the total cortical representation of a given frequency has greater bearing on its predicted discriminability. Our approach is compatible with results like those of Renconzone (1993), which suggest that total cortical representation is the best predictor of behavioral performance following frequency training. However, at the level of cortex, the neural code underpinning frequency discrimination remains an active area of research, and it is likely that a more sophisticated model could provide an even firmer link between the cortical data and individual behavior.

Conclusions

Here we show that early blindness results in narrower tuning for frequency within auditory cortex, providing some of the first evidence for systematic changes in frequency tuning within non-deprived primary auditory cortex as a result of blindness. However, it is not clear whether the changes seen here reflect a developmental adaptation to early blindness, or the ongoing effects of visual deprivation and/or auditory training. Adult PAC has long been held to possess remarkable representational plasticity (Recanzone et al., 1993; Petrus et al., 2014). Thus, future work might address whether adult-onset blindness, short-term visual deprivation, and/or auditory training can alter frequency tuning within PAC, and whether the effects of long-term visual deprivation on auditory

cortex are reversed with the reinstatement of vision, for example, in adult sight-recovery subjects.

CHAPTER 2. Tuning to auditory frequency and motion in human visual cortex after long-term blindness

In collaboration with Fang Jiang and Ione Fine

Here we describe auditory frequency tuning within human middle temporal complex (hMT+) in early blind subjects, which depends upon the presence of motion cues within the stimulus. Stationary pure tones and moving band-pass stimuli produced highly similar tonotopic maps for both early blind and sighted subjects within primary auditory cortex. In hMT+ in early blind subjects, the moving stimulus produced clear evidence for auditory frequency tuning, in contrast to the stationary stimulus. Within hMT+ in sighted subjects, neither the moving nor the stationary stimulus elicited frequency-tuned responses. Thus, after early blindness, hMT+ exhibits selectivity for auditory frequency as well as direction of motion, which may serve to enhance the ability of early blind individuals to segregate individual auditory objects within complex auditory scenes.

INTRODUCTION

Current evidence favors the idea that cross-modal reorganization respects the functional modularity observed in non-deprived cortex. For example, regions associated with visual object processing are implicated in object-size estimation in the congenitally blind (Mahon, 2009), the ventral visual word form area responds during Braille reading (Buchel et al., 1998; Reich et al., 2011), and regions within the occipital dorsal stream - whose activity is linked to visual spatial processing in sighted subjects - are preferentially

active when blind subjects perform a task involving the spatial attributes of auditory and tactile stimuli (Collignon et al., 2011; Renier et al., 2010).

Consistent with this notion of 'functional constancy' (Pascual-Leone & Hamilton, 2001; Pascual-Leone et al., 2005; Saenz et al., 2008), several fMRI studies have demonstrated novel responses to auditory motion in human middle temporal complex (hMT+) in early blind and sight recovery subjects (Bedny et al., 2010; Poirier et al., 2006; Saenz et al., 2008). These responses contain information about the direction of auditory motion (Wolbers et al., 2011), and can be used to predict perceptual decisions about motion direction for ambiguous stimuli in early blind individuals (Jiang et al., 2014). Thus, hMT+ seems intimately tied to the network involved in the perception of auditory motion in blind individuals.

In sighted individuals, neurons in hMT+ have complex receptive fields with properties that include tuning for binocular disparity (DeAngelis & Newsome 1999) as well as direction of motion (reviewed in Britten, 2003, and Born & Bradley, 2005). These properties are thought to be critical for interpreting the motion of objects in space. If hMT+ fills an analogous computational role in the auditory domain, then we might expect that neurons within hMT+ should exhibit complex receptive fields analogous to those observed in visual hMT+.

Auditory frequency provides a salient cue for auditory object segregation (Bregman et al., 1990) and is represented topographically at multiple levels of the auditory system. Therefore, it is plausible that hMT+ might represent auditory frequency, as well as direction of motion, in early blind individuals. Indeed, using a stationary pure tone stimulus, Watkins and colleagues (2013) recently noted that voxels in hMT+ varied

in their frequency preferences in a subset of anophthalmic individuals. However, it was not clear whether these frequency preferences represented genuine frequency tuning. Nor was it clear whether any such frequency tuning might be limited to anophthalmic individuals, in whom under-development of the eyes prevents (exogenous) visual stimulation as well as spontaneous (endogenous) retinal waves during pre-natal development (Stevenson, 2004).

Here, we assessed frequency tuning in auditory and occipital cortex in 4 early blind subjects, 2 sight-recovery subjects, and 6 age-matched controls (see Table 1 for subject details and demographics) using fMRI. To assess frequency tuning, we estimated a population receptive field (pRF) in frequency space for each voxel (Dumoulin & Wandell, 2008; Thomas et al., 2015). When using a pure-tone, stationary stimulus, we observed robust tuning for auditory frequency within primary auditory cortex in all subjects. Within hMT+, we found some evidence for frequency tuning in both early blind and sight-recovery subjects, but not in sighted subjects. These effects were relatively weak, comparable to those previously reported by Watkins and colleagues (2013), and were only observed in a subset of subjects. With a broader-band, moving stimulus, we once again observed robust tuning for auditory frequency within primary auditory cortex in all subjects. In addition, with the moving stimulus, we observed tuning to auditory frequency in hMT+ in both the early-blind and sight-recovery subjects. Frequency tuning bandwidths in hMT+ were similar to those observed in primary auditory cortex in these subjects. Once again, we found no evidence for frequency tuning within hMT+ within any of our sighted controls.

Our data bolster the notion of functional constancy by providing evidence that hMT+ contains information relevant for analyzing the motion of auditory objects in space. Moreover, recruitment of hMT+ occurred not only in early-blind individuals, but also in our sight-recovery subjects, one having had normal visual development up to age three. Thus, in blind individuals, auditory motion processing may be accomplished within a conserved neural architecture that would otherwise support analogous computations relevant for processing visual motion. This selectivity for frequency may serve to enhance the ability of early blind individuals to segregate individual auditory objects within complex auditory scenes.

METHODS

Participants

Four early blind (ages 33-56, 2 males; cause and onset of blindness given in Table 1), two sight-recovery (both age 61, 1 male), and 6 age-matched sighted subjects participated in two sessions of MR imaging. Subjects reported normal hearing and no history of neurological or psychiatric illness. All procedures, including recruitment, consent, and testing, followed the guidelines of the University of Washington Human Subjects Division and were reviewed and approved by the UW Institutional Review Board.

Subject	**Sex**	**Age**	**Clinical description**
EB01	Male	32	Leber's congenital amaurosis, low light perception
EB02	Female	38	Retinopathy of prematurity, no light perception in right eye, minimal peripheral light perception in left eye, 3 months premature
EB03	Female	55	Retinopathy of prematurity, low light perception until retina detached at age 25, 2 months premature
EB04	Male	52	Congenital glaucoma, no light perception
SR01	Male	62	Normal visual development until age 3.5, then blinded in a chemical accident; vision partially restored (postoperative acuity, 20:1000) after a corneal stem cell replacement in the right eye at age 46
SR02	Female	62	Congenital blindness due to retinopathy of prematurity and cataracts; vision partially restored (postoperative acuity, 20:400) after cataract removal in the right eye at age 43

Table 2.1. Subject demographics and clinical descriptions.

Auditory stimulus presentation

Auditory stimuli were generated in MATLAB using custom software and the Psychophysics Toolbox (www.psychtoolbox.org) and were delivered via insert earphones (MR compatible Sensimetrics S86). All stimuli were presented at a sampling rate of 44.1 kHz, with intensities adjusted to ensure flat frequency transmission from 100 Hz to 8 kHz. Subjects were instructed to keep their eyes closed throughout testing, and overhead lighting was switched off.

Stimulus and task

After sound system calibration, stimulus sound intensities were adjusted according to a standard equal-loudness curve created for insert earphones (ISO 226) to approximate equal perceived loudness across frequency. Actual sound intensities (65–83 dB SPL) were matched to the perceived loudness of a 1 kHz tone (reference frequency) at 70 dB SPL. Acoustic noise from the scanner was attenuated by expanding-foam ear-tips, as well as protective earmuffs placed over the ear following earphone insertion. Subjects confirmed that all tones were indeed clearly audible, and of roughly equal loudness across frequency. Tonotopic mapping was carried out using two kinds of stimuli, (1) stationary pure tones and (2) a moving band pass stimulus.

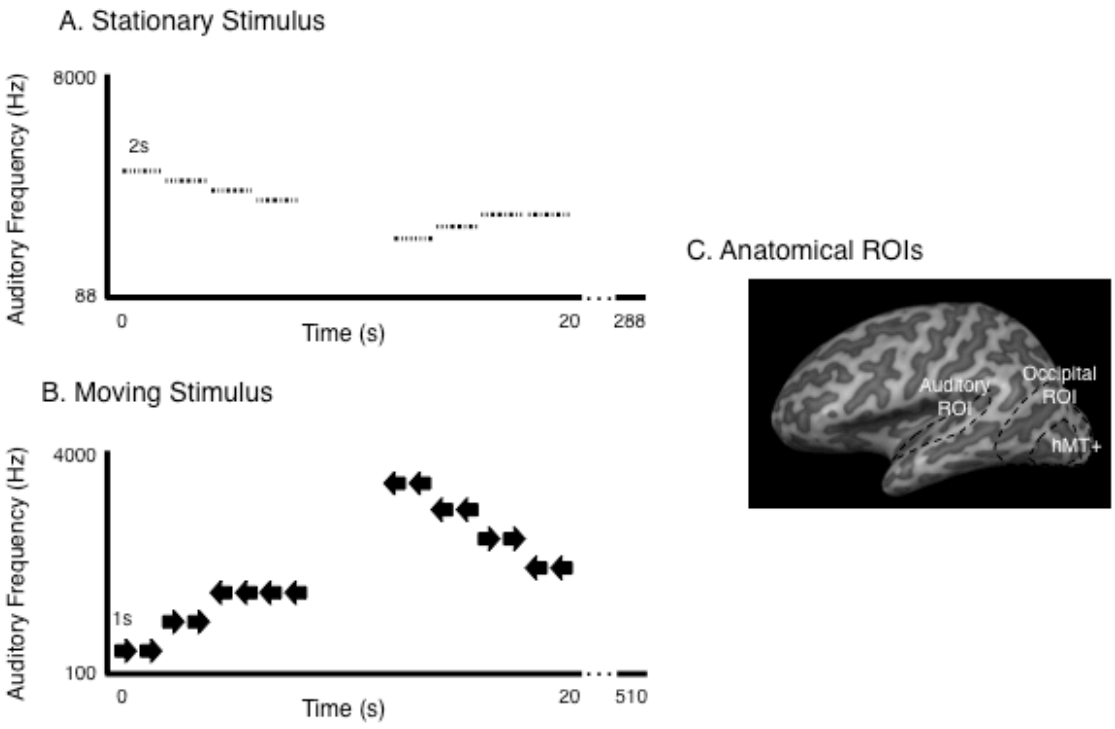

Fig. 2.1. Stimulus schematics and illustration of anatomically defined ROIs. (A) Stationary Stimulus. Each 2s frequency blocks contained 8 pure tone bursts (50 or 200 ms). (B) Moving Stimulus. Each 2s block contained a pair of 1s bursts that both travelled in the same direction, as implied by the arrows. Motion direction varied pseudo-randomly across trials. Motion along the fronto-parallel plane was simulated using both ITD and Doppler shift. (C) Data were analyzed within auditory, occipital, and hMT+ ROIs defined on the cortical surface based on anatomical criteria.

The *stationary* stimulus (Figure 2.1A) contained blocks of pure tone bursts, which varied in auditory frequency (88-8000 Hz, sampled in half octave steps). Each 2s stimulus block contained eight pure tone bursts of the same frequency, presented in a rhythmic pattern to facilitate perceptual segregation of the stimulus from background scanner noise. Each scan consisted of a series of sequences of 3-4 ascending or descending half-octave steps, with the starting frequency and sequence (ascending vs. descending) selected pseudo randomly at the beginning of each sequence. The pseudo

randomization ensured that the distribution of presented frequencies between 88-8000Hz was uniform, and that there were equal numbers of ascending and descending sequences.

The *moving* stimulus (Figure 2.1B) consisted of band pass noise bursts centered at each of 7 frequencies (125-3952 Hz, stimulus bandwidth of approximately 0.8 octaves) in a semi-random order. Each event lasted 2s and contained a pair of 1s bursts travelling at 30 m/sec from left to right, or vice versa, along the fronto-parallel plane. Auditory motion was simulated using ITD and a Doppler shift. Center frequencies for the moving stimulus were selected to occupy the middle to lower end of the audible range to maximize the efficacy of the ITD cue, since thresholds for detecting ITDs are lowest in the range from 700 to 1400 Hz for pure tones (Brughera et al., 2013, Macpherson and Middlebrooks, 2002) and for complex stimuli with carrier frequencies up to roughly 3900 Hz (Henning et al., 1974; Nuetzal & Hafter, 1981).

For both stimulus types, subjects performed a one-back task on the center frequency, responding via button press each time a stimulus block repeated the exact frequency of the previous block (10% of trials).

Magnetic resonance imaging

Acquisition protocol

Functional magnetic resonance images were acquired with a 3T Phillips Achieva scanner (Philips, Eindhoven, Netherlands) at the University of Washington Diagnostic Imaging Sciences Center (DISC) using a 32-channel head coil. Foam padding minimized head motion.

All subjects participated in 2 scanning sessions, 1 for the stationary stimulus, and 1 for the moving stimulus. Sight-recovery subjects completed an additional visual hMT+ localizer scan during the second session. Each session lasted approximately 1 hour. In the *stationary* session, four functional scans were acquired using a standard EPI sequence (36 slices, TR/TE = 2000/25 ms, no slice gap). After discarding the first 5 timeframes, each scan consisted of 255 volumes at an effective voxel size of 3.00 mm isotropic. In the *moving* session, 4 functional scans were acquired using a standard EPI sequence (30 slices, TR/TE = 2000/25 ms, no slice gap). After again discarding the first 5 timeframes, each scan consisted of 144 volumes at an effective voxel size of 2.75 x 2.75 x 3.00 mm (3mm in-plane).

Overhead lighting was switched off during MRI acquisition, and subjects were instructed to keep eyes closed during all scans.

Anatomical voxel selection

For each subject, anatomical regions of interest (ROIs) were selected from the partially inflated left and right hemisphere cortical surface meshes using drawing tools within BrainVoyager QX (Figure 2.1C.)

In auditory cortex, ROI borders were drawn generously to include all voxels within a contiguous region between the lateral border on the crown of the superior temporal gyrus, the medial border within the fundus of the lateral sulcus, the posterior border of the supramarginal gyrus, and the anterior border of the most anterior portion of the temporal lobe.

Within occipital cortex, two ROIs were defined: a large ROI running from the parietal-occipital fissure to the occipital pole, and a smaller ROI within the occipital lobe corresponding to hMT+ as defined using the Julich probabilistic atlas thresholded at 25%. To ensure proper alignment to individual subject anatomical scans, an ROI based on the Julich atlas was first converted into a surface patch at the gray-white matter border of the standard MNI anatomical image. Each subject's individual anatomy was then aligned to the standard MNI surface using cortex based alignment procedures in BrainVoyager. The resulting inverse transformation file was used to project the Julich atlas definition onto each individual subject's cortical surface.

All surface-defined ROIs were mapped back into the brain volume and expanded to include voxels from -1 to 3 mm around the gray-white matter boundary. Preprocessed time-course data for each 3D anatomical voxel within the volume ROIs were then exported to Matlab for further analysis.

Anatomically defined auditory, occipital, and hMT+ ROIs are shown for an example subject in Figure 2.1C.

Pre-processing

For analysis, functional data were resampled into $1 \times 1 \times 1$ mm^3 volumetric space. Standard pre-processing of fMRI data was carried out using BrainVoyager QX software (version 2.3.1 Brain Innovation B. V., Maastricht, The Netherlands), including 3D motion correction and high-pass filtering (cut-off: 3 cycles per scan). Functional data were aligned to the T1-weighted anatomical image acquired in the same session (MPRAGE, $1 \times 1 \times 1$ mm^3). The BrainVoyager QX automatic segmentation routine was

used to reconstruct the cortical surface at the white–gray matter border (with hand-editing to minimize segmentation errors) and the resulting smooth 3D surface was partially inflated.

Population receptive field analysis

Preprocessed fMRI data within the anatomical ROIs were analyzed using methods described in greater detail in CHAPTER 1, and in Thomas et al. (2015). In brief, we assumed that each voxel within an anatomically defined region of interest had a one dimensional Gaussian sensitivity profile on a log auditory frequency axis. Using custom software written in MATLAB, we found, for each voxel, the center (f_0) and standard deviation (σ) of the Gaussian that when multiplied by the stimulus over time and convolved with a hemodynamic response function produced a predicted time course that best correlated with the voxel's measured time course.

After fitting, only voxels that met the following criteria were retained for further analyses: (1) the correlation between the observed fMRI time-course and the time-course predicted by the best-fitting pRF (our goodness-of-fit index) was higher than 0.20 (corresponding to 0.0125 false-discovery rate, based on simulations described below), (2) the center (f_0) of the best fitting pRF fell within the range of tested values (88-8000 Hz for the stationary stimulus, or 100-3162 Hz for the moving stimulus), and (3) the standard deviation (σ) of the best fitting pRF fell between the minimum inter-tone interval and the full presented frequency range, in log frequency.

Statistical analysis

Given the relatively small sample size (n=4 and n=6) used here, we cannot be assured that our data meet the assumptions of parametric tests, and therefore we have opted for a non-parametric approach.

Comparisons of frequency distributions across groups were performed using a bootstrapped $\chi 2$ test of independence. The traditional $\chi 2$ test compares obtained frequency distributions across each group with the expected outcome were distributions independent of group assignment, with a large $\chi 2$ value suggesting that group membership influences frequency distributions (McHugh, 2013). The significance of the $\chi 2$ value was estimated using a bootstrapping procedure implemented with custom software, which simply re-estimated $\chi 2$ after randomly assigning subjects to either group (10,000 simulations) to find the probability of randomized $\chi 2$ values exceeding the obtained $\chi 2$. Subjects (rather than voxels or hemispheres) were randomly assigned between groups.

Statistical significance of group comparisons was estimated using the Wilcoxon rank sum test, a non-parametric test of the equality of population medians based on sample data (Wilcoxon, 1945), which serves as a distribution-free alternative to the two-sample t-test.

RESULTS

Primary auditory cortex

Within auditory cortex, stationary pure tones and moving band-pass stimuli produced similar tonotopic maps for both early blind and sighted subjects and thus provided consistent definitions of PAC. For simplicity, as described in CHAPTER 1, we refer here to the pair of tonotopic gradients comprising hA1 and hR as "primary auditory cortex" (PAC, see p. 17). Figure 2.2 shows frequency centers plotted on the cortical surface along with the boundaries of PAC, defined using the stationary (Figure 2.2A) or moving (Figure 2.2B) stimulus for an example sighted subject. To maximize visual similarity, given that the motion stimulus had a smaller frequency range (100-3162 Hz) than the static stimulus (88-8000 Hz), the color map is restricted to the range of the moving stimulus. Voxels tuned to frequencies below 100 or above 3162 are treated simply as low- or high-pass, for visualization purposes, only.

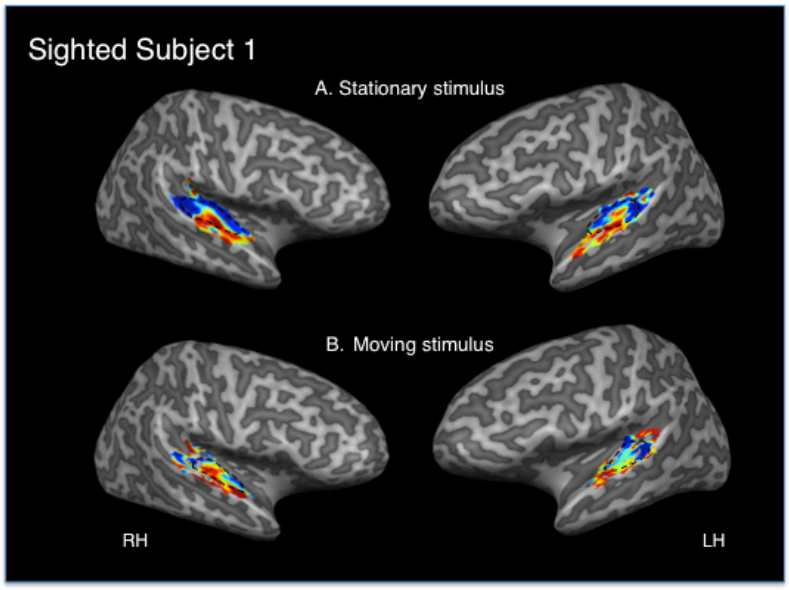

Fig. 2.2. Auditory core (black dashed outline) defined in an example, sighted subject using either the stationary (A) To maximize visual similarity, given that the motion stimulus had a smaller frequency range (100-3162 Hz) than the static stimulus (88-8000 Hz), the color map is restricted to the range of the moving stimulus.

It has previously been shown that PAC can be accurately and consistently defined using pure tones, as well as complex, naturalistic stimuli (Formisano et al., 2011). We similarly found that PAC boundaries were consistent across moving and stationary stimuli. No statistical difference was detected in the size of PAC defined using the moving versus static stimulus (Wilcoxon rank sum test: p=0.4375), although a (non-significant) reduction in the size of PAC as defined using the moving stimulus was observed. This was not surprising, given the smaller frequency range of the moving stimulus. Further, the moving and stationary stimuli were similarly effective at mapping frequency tuning within auditory cortex as a whole. We found no significant difference in the number of voxels fit above threshold within or outside of PAC (within belt and parabelt regions) using the moving versus stationary stimulus (Wilcoxon rank sum test for PAC: p=0.5625; Wilcoxon rank sum test for belt+parabelt: p=1). Finally, we found no significant difference in the surface area of PAC across early blind and sighted subjects for either the static stimulus (Wilcoxon rank sum test: p=0.2500) or the moving stimulus (Wilcoxon rank sum test: p=0.6250).

Figure 2.3, Panels A and B, show histograms of best frequency for the moving stimulus for early blind (blue) and sighted (red) subjects. Distributions for frequency were highly similar across subject groups; bootstrapped χ^2 tests of independence found no effect of early blindness on the distribution of frequency tuning within PAC. Results were similar regardless of whether sight-recovery (SR) subjects were included in the analysis (EB & SR vs. controls: $\chi^2(6,6)=15.0266$, p=0.7608) or ongoing visual deprivation (EB vs. controls: $\chi^2(6,4)=7.7555$, p=0.9418).

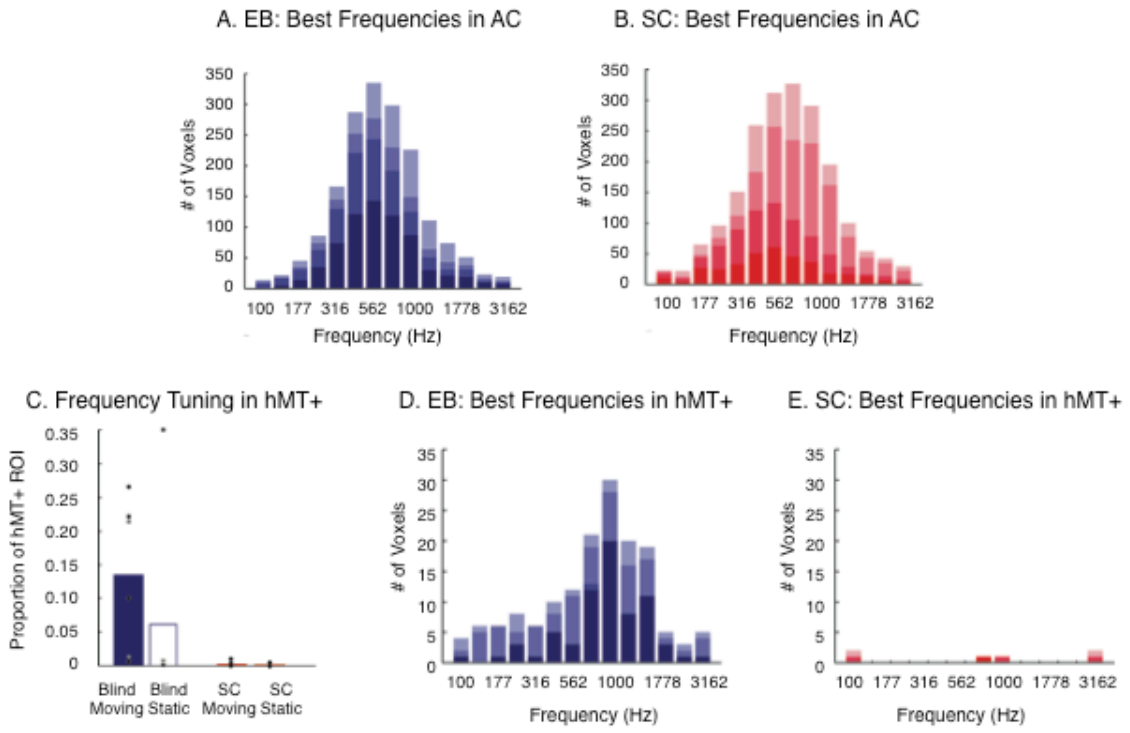

Figure 2.3 Auditory frequency tuning within in auditory cortex and hMT+ ROIs in early-blind, sight-recovery, and control subjects. A-B, Probability histograms of frequency center (f_0) values in auditory cortex, stacked across (A) blind and (B) sighted subjects for the moving stimulus. Colors correspond to the individual subjects. In panel A, early blind subjects are plotted in blue. In panel B, matched control subjects for the early blind group are plotted in red. C, Proportion of voxels within hMT+ probabilistic ROI showing frequency tuning for blind (blue) and sighted (red) subjects using the moving (filled) vs. stationary (unfilled) stimuli. Bars give the group and condition averages, while individual subject data are over-plotted as filled black (early-blind and control subjects) and gray circles (sight-recovery subjects). D-E, Probability histograms of frequency center (f_0) values within hMT+, stacked across (D) blind and (E) sighted subjects for the moving stimulus. Colors correspond to the individual subjects.

hMT+

Figure 2.3C shows the proportion of voxels within hMT+ that showed frequency tuning, for sighted, early blind and sight recovery subjects. No sighted subjects had a significant number of voxels with frequency tuning, for either the stationary or the moving stimulus. In early blind subjects, for the stationary stimulus, frequency tuning

was observed in only 1 out of the 4 subjects. However, robust frequency tuning was evident within hMT+ for the moving stimulus across all four early blind and both sight recovery subjects.

As shown in Figure 2.3C, on average roughly 15% of voxels within our hMT+ ROI showed frequency-tuned responses in blind individuals. Since our anatomical hMT+ ROI was based on a probabilistic atlas, this result provides evidence that frequency tuning overlaps the probable location of hMT+, but it should not be treated as an estimate of the proportion of frequency tuned voxels within hMT+, and may in fact underestimate the proportion of hMT+ exhibiting frequency tuning in any given subject. With sight-recovery subjects, however, it is possible to obtain a functional definition of hMT+. Thus, in this subject group, we were able to assess the prevalence of frequency tuning within hMT+ directly. We defined hMT+ with a traditional moving vs. stationary dot-field localizer, using large dots to insure that the stimulus was visible despite acuity limitations in these subjects. Based on this functional definition, we found that in SR01 46% and within SR02 26% of hMT+ voxels were frequency tuned when using a conservative goodness-of-fit threshold of 0.2 (in sighted subjects almost no voxels within hMT+ passed this goodness-of-fit threshold, as shown in Panel 3C). At a goodness-of-fit threshold of $R > 0.2$, we observe almost no voxels within hMT+ in sighted subjects. Further, based on simulations in which we repeatedly randomized (1000 repetitions) the spatial location of voxels within the whole of occipital cortex and then calculated the proportion of frequency tuned voxels overlapping the hMT+ ROI in sighted subjects, we estimate that $R>0.2$ corresponds to a 1.25% false discovery rate.

Figure 2.3D shows histograms of best frequency within hMT+ for early blind subjects for the moving stimulus. Almost no voxels passed threshold for sighted subjects, as shown in Figure 2.3E. Within blind subjects, the distribution of frequencies was similar to that seen in auditory cortex. Bootstrapped χ^2 tests of independence found no significant difference between the distribution of frequency values in auditory cortex and hMT+ for early blind individuals (χ^2 (6,4)=79.9073, p=0.5435) or sight-recovery subjects (χ^2 (6,2)=175.0236,p=0.0857).

One advantage of the pRF method is that it provides an estimate of tuning width as well as best frequency for each voxel. Figure 2.4 shows tuning width estimates, using the moving stimulus, for sighted subjects in PAC, and early blind subjects in both PAC and hMT+. As shown previously using stationary pure-tone stimuli (discussed in greater detail in Chapter 1), tuning widths in PAC were narrower within early blind individuals compared to sighted subjects (Wilcoxon rank sum test: $p<0.001$). This effect held when sight-recovery subjects were included in the blind group (Wilcoxon rank sum test: p=0.0469). Tuning width estimates for early blind hMT+ were similar to those obtained in auditory cortex.

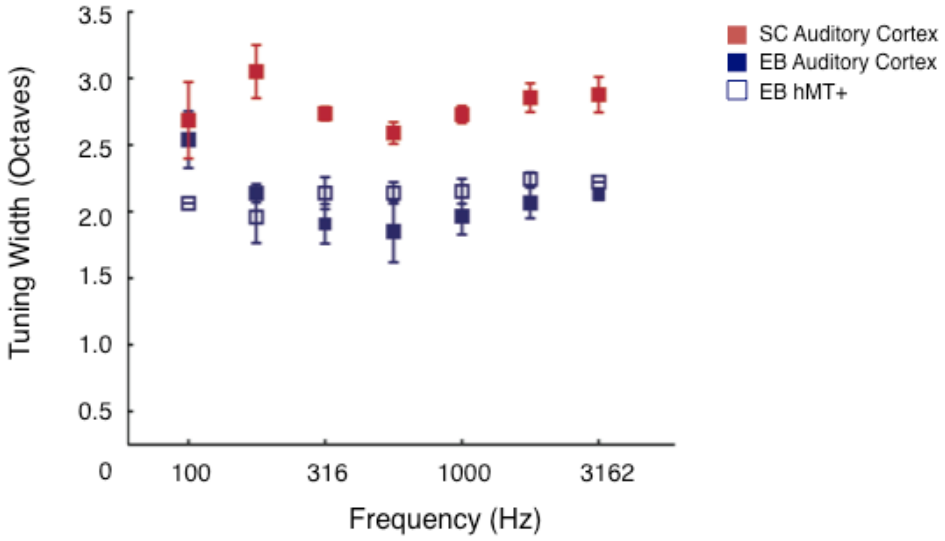

Figure 2.4. PRF tuning width as a function of frequency. Voxels were sorted into the half-octave bins based on their best-frequency values. Mean tuning width calculated for each bin, separately for the hMT+ and PAC ROIs. Filled squares represent auditory cortex, open squares hMT+. Early-blind subjects, plotted in blue, show narrower tuning to auditory frequency within both PAC and hMT+, relative to sighted PAC.

Figure 2.5 shows best frequency and tuning widths within hMT+ plotted on the cortical surface for each early blind subject. In 2 of our 4 subjects we find voxels tuned across much of the tested frequency range, while in the other two subjects voxels were clustered within a more narrow frequency range. In both sight-recovery subjects, we again see voxels tuned across much of the frequency range. However, we see little evidence of a consistent tonotopic organization across subjects.

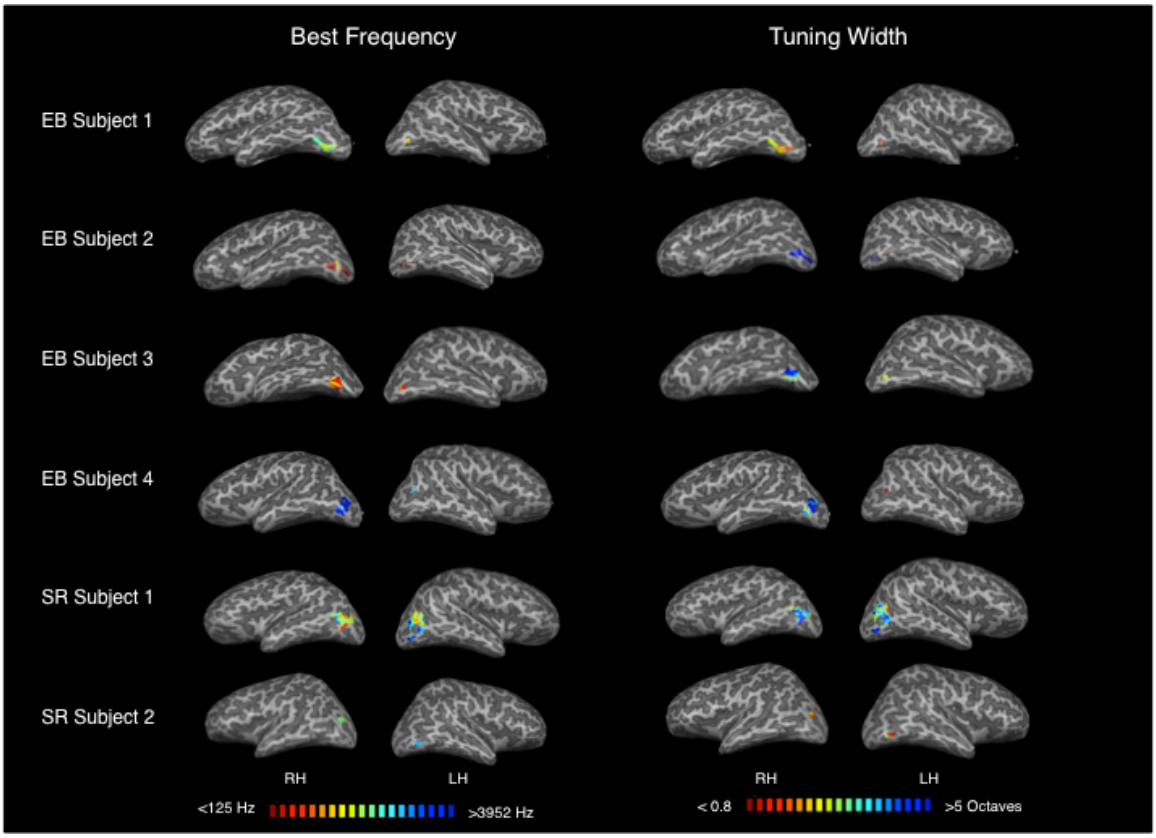

Figure 2.5. Best frequency (A) and tuning widths (B) within hMT+ plotted on the cortical surface for each early blind subject and sight-recovery subject. Here, hMT+ is defined using the Julich probabilistic atlas, as described in the main text. Frequency center values are color-coded along a gradient, with red corresponding to the lowest frequency value (125 Hz) through blue corresponding to the highest frequency (3952 Hz). Tuning width values are color-coded along a gradient with red corresponding to the narrow tuning (0.8 octaves) through blue corresponding to broader tuning (5 octaves). All maps are thresholded at R > 0.2.

DISCUSSION

Here, we assessed frequency tuning in auditory and occipital cortex in 4 early blind subjects, 2 sight-recovery subjects, and 6 age-matched controls using fMRI and a pRF model with two stimulus types: (1) pure tones, and (2) band pass noise with simulated motion along the horizontal plane. Using a pure tone, stationary stimulus similar to that of Watkins et al. (2013), we observed tuning for auditory frequency within primary auditory cortex in all subjects. Within hMT+, we found some evidence for frequency tuning in both early blind and sight recovery subjects, but not in sighted subjects. In early blind subjects, for the stationary stimulus, frequency tuning was observed in only 1 out of the 4 subjects. Similarly, Watkins and colleagues only observed frequency preferences in hMT+ in 2 out of 5 of their anophthalmic subjects using a stationary stimulus. However, robust frequency tuning was evident within hMT+ for the moving stimulus across all four early blind and both sight-recovery subjects, but none of the sighted controls. Finally, the band pass, moving stimulus proved to be as suitable as the pure tone stimulus for measuring frequency tuning within PAC in all subjects.

Functional constancy

A currently influential framework suggests that cortex can be characterized in terms of "functional constancies", or a "meta-modal" organization (Pascual-Leone & Hamilton, 2001; Pascual-Leone et al., 2005), in which brain areas serve fixed computational roles, regardless of input modality. One of the most frequently cited examples is that of hMT+, which in blind humans appears to trade visual for auditory input, while continuing to serve as part of a network computing direction of motion

(Jiang et al., 2014; Wolbers et al., 2011; Bedny et al., 2010; Poirier et al., 2006; Saenz et al., 2008). Beneath the intuitive appeal of this framework lies a remarkable claim: Visually driven neurons hMT+ have complex receptive fields that aid in segmentation of visual objects and surfaces (e.g., strength of surround suppression in hMT+ depends on location in depth (Bradley & Andersen 1998)). Thus, for hMT+ to serve an analogous role in the auditory domain, it should contain information relevant for segmenting auditory objects.

Auditory frequency provides a salient cue for grouping auditory objects, based, for example, on harmonic structure (see Griffiths & Warren, 2003, and Bizley & Cohen, 2013 for reviews). Our finding of frequency tuning within hMT+ in blind individuals is compatible with the view that auditory motion processing may be accomplished within a conserved neural architecture that would otherwise support analogous computations relevant for processing visual motion. Future tests of auditory receptive field properties in hMT+ may further strengthen the argument for functional constancy, or may instead reveal limitations of the analogy.

Interdependence of auditory frequency and motion processing

Of course, co-localization of auditory frequency and direction tuning within hMT+ does require that the same neural populations represent both features; it merely leaves open the possibility. In sighted individuals, auditory motion direction and auditory frequency representations are, in fact, not independent. The auditory motion aftereffect (MAE) is reduced when adapting and test stimuli differ in frequency content (Grantham, 1998) by as little as 1 octave (Dong et al., 2000). This frequency dependence resembles

the dependence on retinal location classically observed for the visual MAE (Wohlgemuth, 1911), and suggests that these features may be jointly encoded.

The planum temporale (PT) has been linked to auditory motion processing in sighted individuals (e.g., Lewis, et al., 2000; Alink et al., 2012; Jiang et al., 2014), and this area generally shows auditory frequency preferences without clear tonotopic organization (i.e., lacking the tonotopic gradient seen in PAC; e.g., Langers et al., 2007). This pattern is reminiscent of our findings in blind hMT+ (tuning to auditory frequency, without a clear tonotopic gradient), and is compatible with the idea that in early blind individuals, hMT+ is part of the perceptual network representing auditory motion, perhaps even usurping the function of PT (Jiang et al., 2014).

Visual and auditory motion processing co-exist with auditory frequency tuning in adult-sight recovery subjects

In addition to the early-blind subjects, we tested two adult sight-recovery subjects who were previously shown to have auditory motion responses within hMT+ (Saenz et al., 2008). With these individuals, it was possible to obtain a precise functional definition of hMT+, which allowed us to assess the prevalence of frequency tuning within hMT+ directly.

Moreover, including these subjects allowed us to ask whether early and/or sustained blindness might be required for the appearance of auditory frequency tuning I hMT+. As described elsewhere (Fine et al., 2003; Saenz et al., 2008) one of these subjects had normal visual experience up to age 3, at which stage his visual motion processing should have been fairly mature (Maurer and Lewis, 2005). Thus it appears

that congenital or very early blindness is not strictly required for auditory frequency tuning to emerge. One possibility is that hMT+ inherits a representation of both auditory space and frequency via reorganization of subcortical inputs, as suggested by Watkins et al. (2013). If subcortical reorganization is necessary for auditory frequency selectivity within hMT+, then these connections must retain plasticity until at least age 3. Alternatively, frequency tuning in hMT+ may be mediated by cortico-cortical connections or feedback from heteromodal cortical areas (Bedny et al., 2010).

Finally, the presence of auditory frequency tuning in hMT+ in these subjects suggests that frequency selectivity can co-exist with visual motion processing. Again, while the co-localization of auditory and visual motion responses is intriguing, it should be noted that our analysis of the BOLD response cannot be used to infer that the same neural circuits underlie visual and auditory motion processing in these individuals: The relevant neural populations may simply overlap at the relatively coarse spatial scale of fMRI. Future work employing, for example, behavioral adaptation methods, should lend further insight into the extent of cross-modal allocation of neural resources in these individuals

Conclusions

Using a moving stimulus, we observed auditory frequency tuning within hMT+ in four early blind and two sight-recovery subjects, but none of our sighted controls. Thus, after early blindness, hMT+ exhibits selectivity for auditory frequency as well as direction of motion. Further, auditory frequency tuning is present even after successful sight-recovery, suggesting that this function can co-exist with visual motion processing.

Thus, we suggest that tuning to auditory frequency must arise via connections that retain plasticity into early childhood, without the disruption of existing feed-forward visual inputs to hMT+. This selectivity for frequency may serve to enhance the ability of early blind individuals to segregate individual auditory objects within complex auditory scenes.

CHAPTER 3. Stability of visual cortical organization and perception after long-term blindness and sight-recovery

In collaboration with Jason M. Webster (joint first author) and Ione Fine
Manuscript published in Psychological Science, 2015

In 2000, monocular vision was restored to M.M., who had been blind between the ages of 3 and 46 years. Tests carried out over 2 years following the surgery revealed impairments of 3-D form, object, and face processing and an absence of object- and face-selective blood-oxygen-level-dependent responses in ventral visual cortex. In the present research, we reexamined M.M. to test for experience-dependent recovery of visual function. Behaviorally, M.M. remains impaired in 3-D form, object, and face processing. Accordingly, we found little to no evidence of the category-selective organization within ventral visual cortex typically associated with face, body, scene, or object processing. We did observe remarkably normal object selectivity within lateral occipital cortex, consistent with M.M.'s previously reported shape-discrimination performance. Together, these findings provide little evidence for recovery of high-level visual function after more than a decade of visual experience in adulthood.

INTRODUCTION

M.M. was 3.5 years old in 1960 when a chemical explosion caused the loss of his left eye and blindness in his right as a result of corneal damage. As described previously (Fine et al., 2003), M.M. had some perception of light but no experience of contrast or form over a period of 43 years. He reported no visual memories or imagery, despite one unsuccessful corneal replacement attempt in childhood. In 2000, M.M. received a corneal

transplant and stem cell therapy, which restored vision in his remaining eye. In tests carried out over the first 2 years after surgery, M.M. showed severe amblyopia (an acuity limit of ~1.2 cycles per degree, corresponding to Snellen acuity of ~20/500) and substantial deficits in high-level visual processing (Fine et al., 2003). In the work reported here, we used behavioral measures and functional MRI (fMRI) to assess whether M.M.'s processing of complex form, objects, and faces has changed after more than 10 years of restored sight.

Most cases of early visual deprivation are due to congenital cataracts that are generally diagnosed and removed within the first year of life. Thus, these cases differ substantially from that of M.M., who was blinded at the age of 3.5 years and remained blind for much of his adult life. Indeed, M.M.'s period of deprivation and the period found in more traditional examples of bilateral cataracts are practically non-overlapping. Infants treated for congenital cataracts early in life regain useful visual function, though deficits in a variety of low-level (Maurer, Mondloch, & Lewis, 2007), mid-level (Ellemberg et al., 2005; Lewis et al., 2002), and high-level (Le Grand, Mondloch, Maurer, & Brent, 2004; Robbins, Nishimura, Mondloch, Lewis, & Maurer, 2010) capacities remain. It is clear that the period of visually driven normal development differs from both the sensitive period for damage and the sensitive period for recovery, and that these developmental windows differ substantially across various types of visual processing (Lewis & Maurer, 2005) and depend upon a complex balance between inhibitory and excitatory circuits that are themselves affected by deprivation (Bavelier, Levi, Li, Dan, & Hensch, 2010).

At present, some uncertainty exists in the literature as to whether people whose sight is restored in adulthood can regain useful vision and over what timescale such improvement might occur. Previous studies and case reports ((Cheselden, 1727) Fine et al., 2003; Gregory & Wallace, 1963; Šikl et al., 2013; Sinha & Held, 2012; Valvo, 1971) suggest that adults who have recovered their sight tend to find the visual world confusing and difficult to interpret even many months after surgery, although certain visual abilities seem to improve after surgery (Kalia et al., 2014; Ostrovsky, Meyers, Ganesh, Mathur, & Sinha, 2009), and some spared high-level visual function has been reported in one case of sight recovery in early adolescence (Ostrovsky, Andalman, & Sinha, 2006).

When tested shortly after surgery, M.M. had normal perception of color and motion, and only modest deficits in perception of simple form (Fine et al., 2003), consistent with the comparatively early sensitive periods proposed for these capacities. In contrast, M.M. showed severe deficits in many aspects of complex form, object, and face processing, accompanied by a lack of category-selective responses for faces or objects within ventral visual cortex, as measured using fMRI. Although these capacities are qualitatively present at 3 to 4 years of age, when M.M. lost vision, certain aspects of object and face processing continue to develop well into early childhood (Lewis & Maurer, 2005; McKone, Crookes, Jeffery, & Dilks, 2012; Nishimura, Scherf, & Behrmann, 2009), and the degree of plasticity within these areas after early childhood has not yet been established in humans. Thus it remains possible that M.M. could have recovered these capacities with sufficient visual experience.

METHODS

Subjects

M.M. and 2 age- and gender-matched control subjects participated in both the behavioral and fMRI portions of the experiment. Two additional control subjects were excluded from the analysis because they fell asleep during the fMRI portion of the experiment. All procedures, including recruitment and testing, followed the guidelines of the University of Washington Human Subjects Division and were approved by the institutional review board. All subjects provided informed consent.

Procedure for behavioral experiments

Because M.M. had studied the original object and face stimuli and received feedback after the original experiments (Fine et al., 2003), different databases were used in the experiments described here to obtain novel but analogous stimuli. Object identification and emotion classification were tested using gray-scale images adapted from a standard stimulus set courtesy of Michael J. Tarr, Center for the Neural Basis of Cognition and Department of Psychology, Carnegie Mellon University (http://www.tarrlab.org/). Gender classification was tested using stimuli adapted from the Stirling face set (http://pics.stir.ac.uk/2D_face_sets.htm). To ensure that M.M. was familiar with the objects in our stimuli, we selected common household items to which he was regularly exposed. We chose novel face stimuli in which the number of nonconfigural cues, such as eyebrow shape and hair-length, was minimized; M.M. had previously reported using such cues to discriminate male from female faces.

All stimuli were presented on a large flat-screen monitor, which subtended 56 × 42 degrees of visual angle at a viewing distance of 35 cm. Stimulus images subtended roughly 12° and were presented in gray scale on plain, achromatic backgrounds. As in our original experiments (Fine et al., 2003), M.M. viewed unblurred stimuli, whereas control subjects viewed stimuli that were convolved with a Gaussian filter centered at 1 cycle per degree to match M.M.'s psychophysically determined acuity. See Fig. 3.1. M.M.'s acuity has remained stable since the initial tests conducted shortly after he recovered his sight (Fine et al., 2003; Levin, Dumoulin, Winawer, Dougherty, & Wandell, 2010). For all tasks, we chose the number of trials to run per task prior to the start of data collection to allow presentation of several exemplars from each category while minimizing fatigue in M.M., for whom the tasks were challenging.

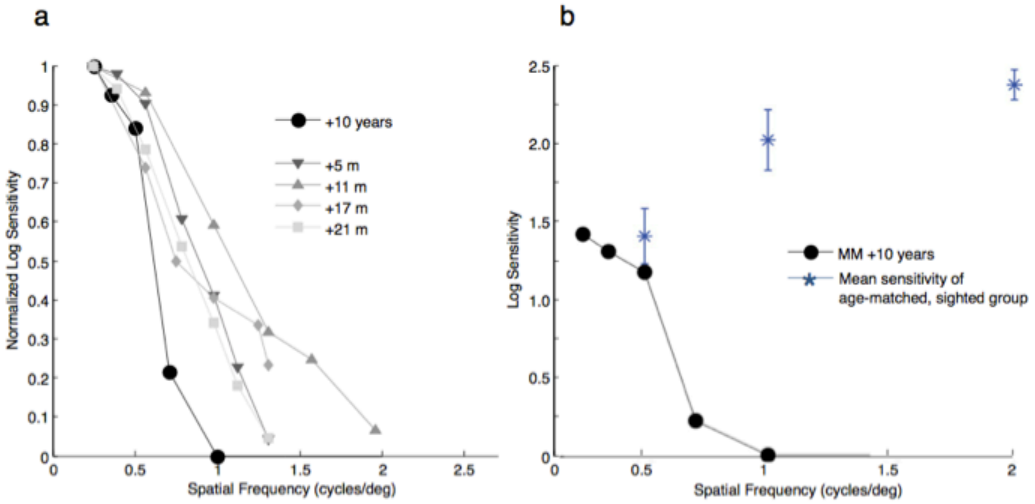

Figure 3.1. Contrast sensitivity in MM 11 months to 10 years post-surgery (a): Large black symbols represent MM's normalized sensitivity as a function of spatial frequency measured psychophysically using a two alternative forced-choice over 10 years after surgery. Smaller gray symbols represent MM's normalized sensitivity measured psychophysically using a method of adjustment 5-21 months after surgery, data re-plotted from Fine et al. (2003). It is not clear whether the loss in apparent sensitivity is due to changes in MM's optics, changes in equipment (e.g. a brighter monitor) or the

changes in psychophysical procedure from adjustment to forced choice. The small deterioration in his measured CSF did not result in a discernible quality difference in the blurred photographs presented to control subjects. CSF in MM compared with an age-matched sighted group: Large black symbols represent MM's sensitivity (un-normalized), alongside average sensitivity values measured in a group of normally sighted subjects in their 50s, re-plotted from Owlsey et al. (1982). Error bars reflect standard deviation.

To assess perception of complex 3-D form, we presented subjects with line drawings of cubes that were intact, had a single line missing, or were rearranged to disrupt the 3-D structure while preserving local junctions. Subjects completed 32 trials, in total. On each trial, a stimulus was presented for 4 s, followed by an unlimited response interval. Subjects were asked to report via key press whether each image depicted a cube or a jumbled shape.

To further test perception of simple shape and 3-D form, we adapted a set of stimuli containing images of 3-D forms photographed from various viewpoints spanning a 360° rotation (Scharff, Palmer, & Moore, 2013). To create a version of the task that did not require interpolation in depth, we modified a subset of the stimuli by tracing their outer contours and then filling them with a uniform gray (see Fig. 1 for example stimulus images). Subjects matched 3-D images across rotations in depth and 2-D images across rotations in the x-y plane. There were 60 trials in each condition. Stimuli remained on screen until subjects pressed one of two keys to report whether two images, shown simultaneously on the left and right halves of the display, contained rotated versions of the same object or different objects. All subjects completed the 2-D version of the task first.

For the object-identification task, subjects were asked to verbally identify each of 41 unique items, advancing to the next trial by pressing a key when they were unsure of

an object's identity. Gender (male, female) and emotion (happy, neutral, sad) classification were tested via two- and three-alternative forced-choice paradigms, respectively. The gender-classification task consisted of 40 trials (20 faces of each gender) and the emotion-classification task consisted of 45 trials (15 individuals displaying each emotional expression). As with the shape stimuli, face and object stimuli were presented individually for 4 s at the center of the display, and subjects had unlimited time to respond by pressing a key.

Procedure for fMRI experiment

Category-selective regions in the ventral visual pathway have been well characterized in subjects who have normal sight (Kanwisher & Dilks, 2013). To ensure that any absence of this organization in M.M. could not be attributed to his reduced acuity, we showed control subjects blurred as well as unblurred versions of the stimuli. Subjects viewed stimuli presented on a screen at the end of the scanner bore via a mirror attached to the head coil. Cortical category-selective blood-oxygen-level-dependent (BOLD) responses were estimated using freely viewed, colorful, full-screen 3-s video clips presented using a block design that alternated between faces, bodies, scenes, objects, and scrambled objects (Julian, Fedorenko, Webster, & Kanwisher, 2012). Face, body, and object videos were recorded against a black background. Scene stimuli consisted mostly of rural locations and included buildings, yards, and forested roads. To create scrambled versions of the object stimuli, we segmented each object clip into a 15 × 15 grid, and spatial locations were shuffled in a pseudorandom order. Example frames are shown in Figure 3.2.

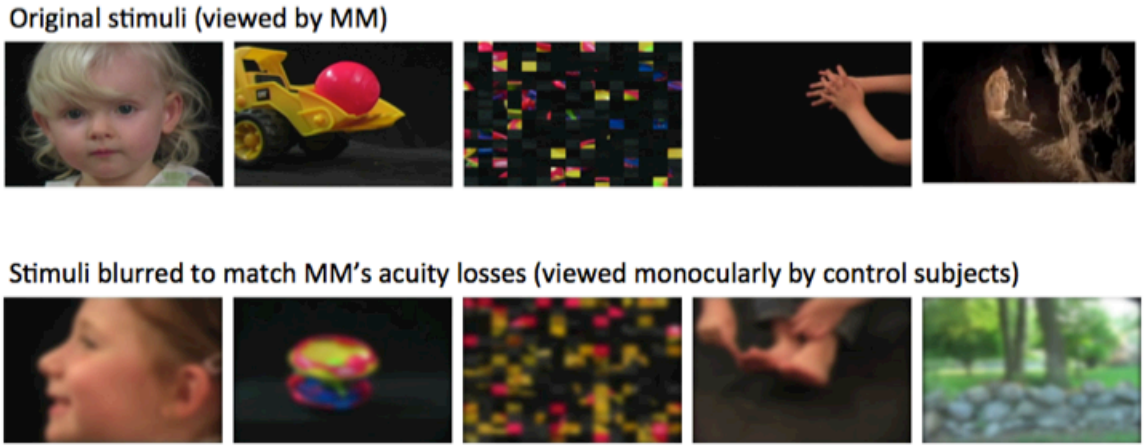

Figure 3.2. Example frames from the video clips used to examine category-selective BOLD activity.

Each block lasted 18 s and consisted of six clips. Uniformly colored screens were used as a baseline and were presented at the beginning, middle, and end of each run. The blocks of movie clips in each run were presented in a palindromic order (e.g., one order used was cFSOBGcGBOSFc, where F = faces, B = bodies, S = scenes, O = objects, G = grid-scrambled objects, and c = uniformly colored screens). Each subject completed eight 234-s runs. Control subjects first completed four runs with an eye patch over the left eye. In these runs, the stimuli were blurred with a Gaussian filter to match M.M.'s psychophysically determined acuity. In the following four runs, control subjects binocularly viewed unblurred stimuli, which allowed us to directly assess the effects of blurring and monocular viewing on category-selective organization. M.M. always viewed unblurred stimuli with his remaining (right) eye.

Scanning was performed using a 3T Allegra scanner with a 32-channel head coil at the Diagnostic Imaging Sciences Center at the University of Washington. High-resolution T1-weighted magnetization-prepared rapid-acquisition gradient-echo images were collected in 128 sagittal slices (repetition time (TR) = 7.6 ms, echo time (TE) = 3.5 ms, voxel size = 1 mm isotropic). BOLD images were acquired with a gradient-echo echo-planar image sequence (TR = 1,500 ms, TE = 25 ms, flip angle = 75°, field of view = 220 × 220, voxel size = 3 mm isotropic). The acquisition window was positioned off axial to include the temporal and occipital lobes.

Structural MRI data were analyzed with FreeSurfer (Version 5.2; http://surfer.nmr.mgh.harvard.edu/) to construct cortical surface models for each subject. FsFast (Version 5.2; https://surfer.nmr.mgh.harvard.edu/fswiki/FsFast) was used to process fMRI data. Preprocessing involved motion correction using the 3dvolreg algorithm in the Analysis of Functional and Neural Images (AFNI) software suite (Cox & Jesmanowicz, 1999) and the FMRIB Software Library Brain Extraction Tool (Smith, 2002). Each functional run was then registered to that subject's cortical surface model using boundary-based registration (Greve & Fischl, 2009). A general linear model was used to estimate the cortical response to each experimental condition. Statistical contrasts were computed for faces versus objects, objects versus scrambled objects, bodies versus objects, and scenes versus objects. Contrast maps were assessed at a threshold of $|p| < .0001$, uncorrected, prior to further analyses, similar to numerous previous studies of the ventral visual stream (Downing, Jiang, Shuman, & Kanwisher, 2001; Epstein & Kanwisher, 1998; Kanwisher & Dilks, 2013; Kanwisher, McDermott, & Chun, 1997; Malach et al., 1995). Data were not smoothed or normalized to a template.

RESULTS

Behavioral experiments

M.M. discriminated images of cubes from incomplete and scrambled versions with accuracy greater than chance level, but his performance was significantly below the performance of control subjects, which suggests that M.M. has continued impairment in 3-D form perception. Similarly, M.M.'s performance on a simple 2-D rotation task was higher than expected from chance alone, but significantly worse than control subjects' performance. When required to match 3-D forms at varying rotations in depth, M.M.'s performance was indistinguishable from chance and significantly below the performance of control subjects. M.M. correctly named several household objects, though significantly fewer than did control subjects, for whom the task was trivial. For both the gender- and emotion-classification tasks, M.M.'s performance was significantly worse than the performance of control subjects and not distinguishable from chance. Finally, M.M. showed no significant improvement in performance between 2003 and 2013 for any of the tasks. See Table 3.1 and Figure 3.3 for a summary of these results.

Table 1. M. M.'s Performance in the Six Behavioral Tasks Compared With Chance, Control Subjects' Performance, and M. M.'s Prior Performance

Comparison	Object recognition	Face classification: gender	Face classification: emotion	2-D shape constancy	3-D shape constancy	3-D shape recognition
M. M. vs. chance	—	.075 [−.14, .29]	.11 [−.085, .31]	.16* [.035, .28]	.12 [−.0081, .24]	.33** [.095, .56]
M. M. vs. control subjects	−.66** [−.81, −.51]	−.43** [−.58, −.27]	−.34** [−.53, −.16]	−.21** [−.32, −.11]	−.20** [−.31, −.088]	−.31** [−.49, −.14]
M. M. 2013 vs. M. M. 2003	.067 [−.15, .28]	−.13 [−.35, .099]	−.16 [−.41, .082]	—	—	—

Note: The table presents the difference in the proportion of correct responses and the corresponding 95% confidence intervals.
*$p < .05$. **$p < .01$.

Table 3.1. M.M.'s Performance in the Six Behavioral Tasks Compared With Chance, Control Subjects' Performance, and M.M.'s Prior Performance.

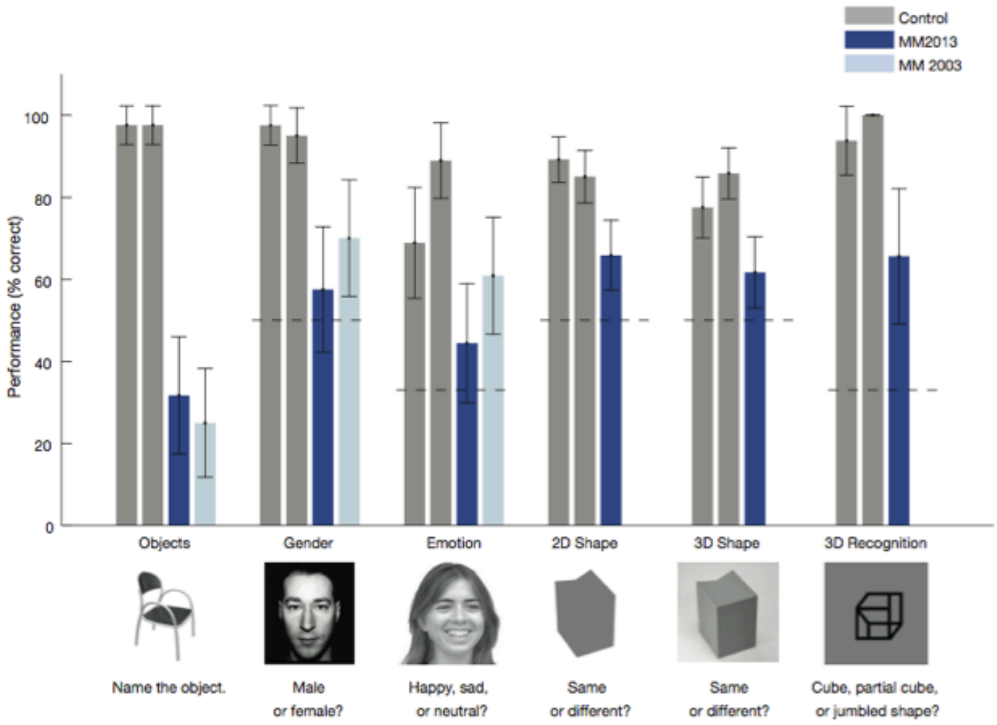

Figure 3.3. Mean percentage of correct responses as a function of stimulus category. Results are shown separately for each control subject, for M.M. in 2013, and for M.M. in 2003. An example unblurred stimulus image is shown for each category; however, in this experiment, all stimuli shown to control subjects were blurred to match M.M.'s visual-acuity losses. Where applicable, chance performance is indicated with a dashed line. Error bars represent 95% confidence intervals.

fMRI experiments

Control subjects' responses to monocularly viewed, blurred stimuli and binocularly viewed, unblurred stimuli were qualitatively similar (data for the latter are not reported).

Face and object selectivity.

Consistent with previous research (for a review, see Kanwisher & Dilks, 2013), our results showed that control subjects had robust category-selective responses for faces and objects within lateral occipital and ventral temporal cortex. Figures 3.4a and 3.4b show data from 1 control subject (four runs with blurred, monocularly viewed stimuli; data from the other control subject are in Fig. 3.5). As expected, a contrast between faces and objects (Fig. 3.4a) isolated face-selective regions in the lateral occipital cortex (LOC), superior temporal sulcus, and fusiform gyrus in both control subjects. Similarly, a contrast between objects and scrambled objects revealed a typical pattern of object-selective regions (Fig. 3.4b).

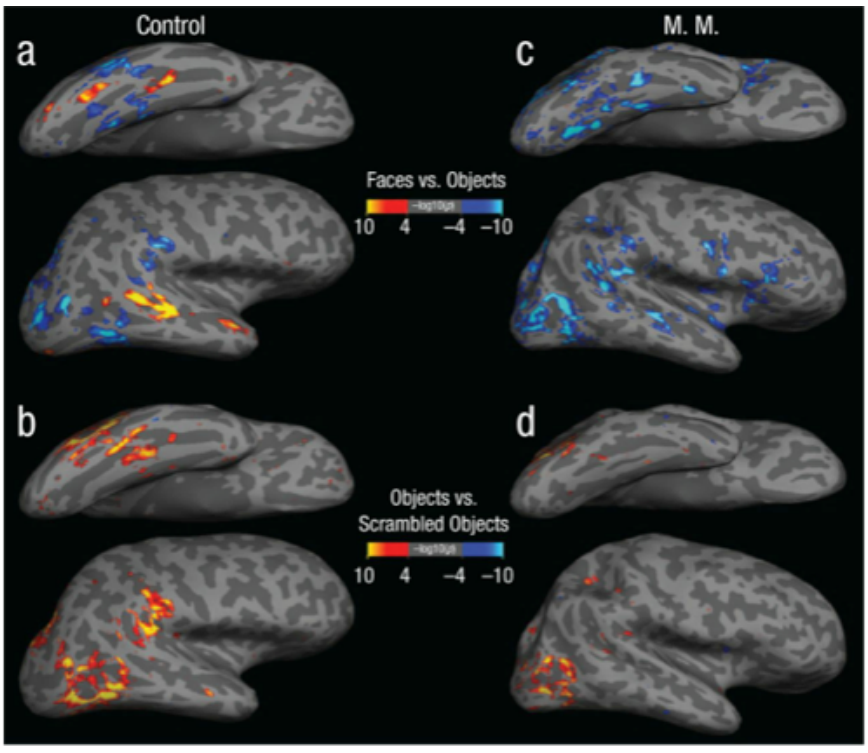

Figure 3.4. Ventral and lateral views of inflated right hemispheres showing results of the contrasts between faces and objects (a, c) and between objects and scrambled objects (b, d). Results are shown separately for 1 control subject (left column) and for M.M. (right column). Data were averaged across four scans (in which stimuli were blurred and monocularly viewed) for the control subject and eight scans for M.M. Results are displayed at a threshold of $|p| < .0001$.

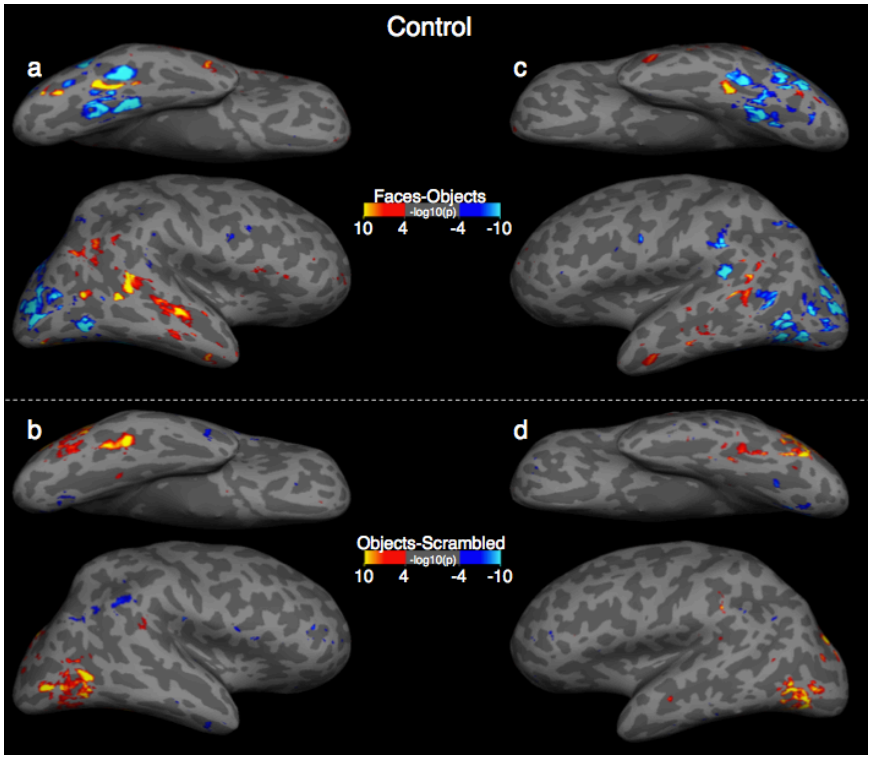

Figure 3.5. Ventral and lateral views of inflated cortical hemispheres showing results of the contrasts between faces and objects (a, c) and objects and scrambled objects (b, d) for the second control subject. Data were averaged across four scans (in which stimuli were blurred and monocularly viewed). Results are displayed at a threshold of $|p| < .0001$.

In contrast, M.M. showed no evidence of face selectivity, even after more than a decade of recovered sight (Fig. 3.4c). While some regions in ventral temporal cortex responded more to objects than to faces, these regions did not show a selective response to objects in a contrast between objects and scrambled objects (Fig. 3.4d), which suggests that M.M. also lacks typical high-level object-selective cortical responses. With a very lenient threshold, there was some evidence for a highly attenuated object-selective response in the ventral temporal cortex, though this potential activity was not clearly differentiable from noise.

M.M. did show object-selective activity in the contrast of objects versus scrambled objects on the lateral surface in a location consistent with the object-selective region LOC. Given that M.M. has no difficulty discriminating different 2-D shapes (Fine et al., 2003), this finding is compatible with those of previous studies suggesting that LOC encodes shapes without being involved with matching those shapes to stored object representations (Grill-Spector et al., 1999; Kanwisher & Dilks, 2013; Kourtzi & Kanwisher, 2001; Malach et al., 1995), though we caution that our finding of relatively intact responses in LOC should not be taken as evidence for fully functional shape encoding.

Scene selectivity.

The contrast of scenes versus objects did not yield the expected results in our control subjects. Monocular viewing of blurred stimuli produced attenuated responses in the right parahippocampal cortex of 1 subject (Fig. 3.6b), although this subject had a robust response in the left hemisphere (see Fig. 3.7b). In a second control subject, we found very little scene-selective response for the blurred stimuli (see Figs. 3.8b and 3.8d). Both of these subjects showed typical responses to unblurred stimuli. It is possible that the lack of scene-selective response, particularly in the parahippocampal place area, results from a high-spatial-frequency bias in this region (Rajimehr, Devaney, Bilenko, Young, & Tootell, 2011). M.M. showed no scene-selective responses in either the lateral occipital or ventral temporal cortex (Fig. 3d) in either hemisphere (Fig. 3.7). At a lower threshold, we observed a small region consistent with the parahippocampal place area

that responded slightly more to scenes than to objects, though this potential activity was not clearly differentiable from noise.

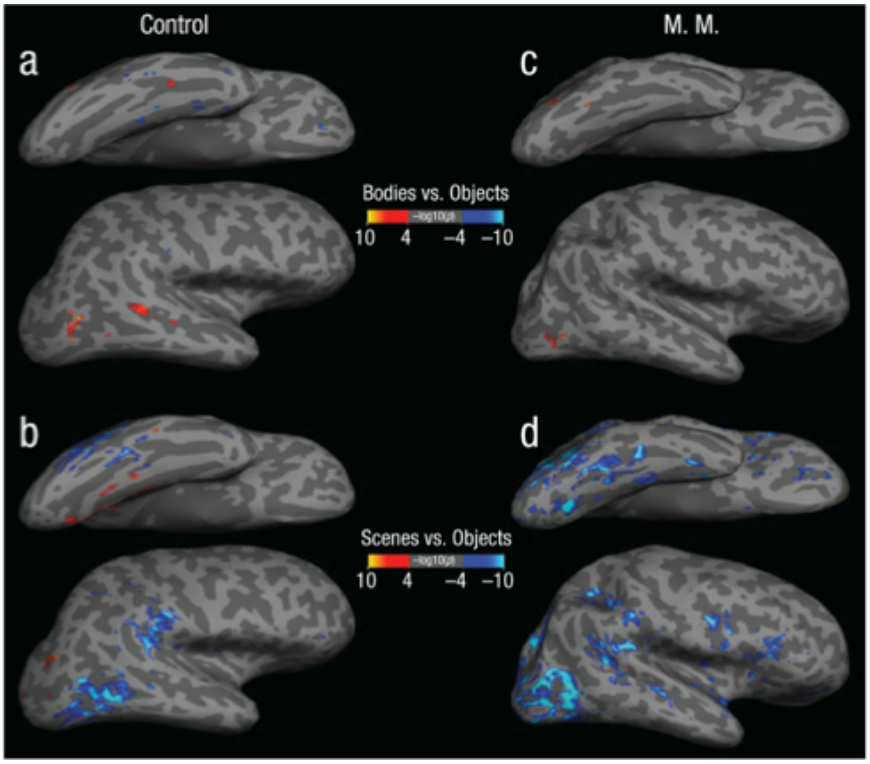

Figure 3.6. Ventral and lateral views of inflated right hemispheres showing results of the contrasts between bodies and objects (a, c) and between scenes and objects (b, d). Results are shown separately for 1 control subject (left column) and for M.M. (right column). Data were averaged across four scans (in which stimuli were blurred and monocularly viewed) for the control subject and eight scans for M.M. Results are displayed at a threshold of $|p| < .0001$.

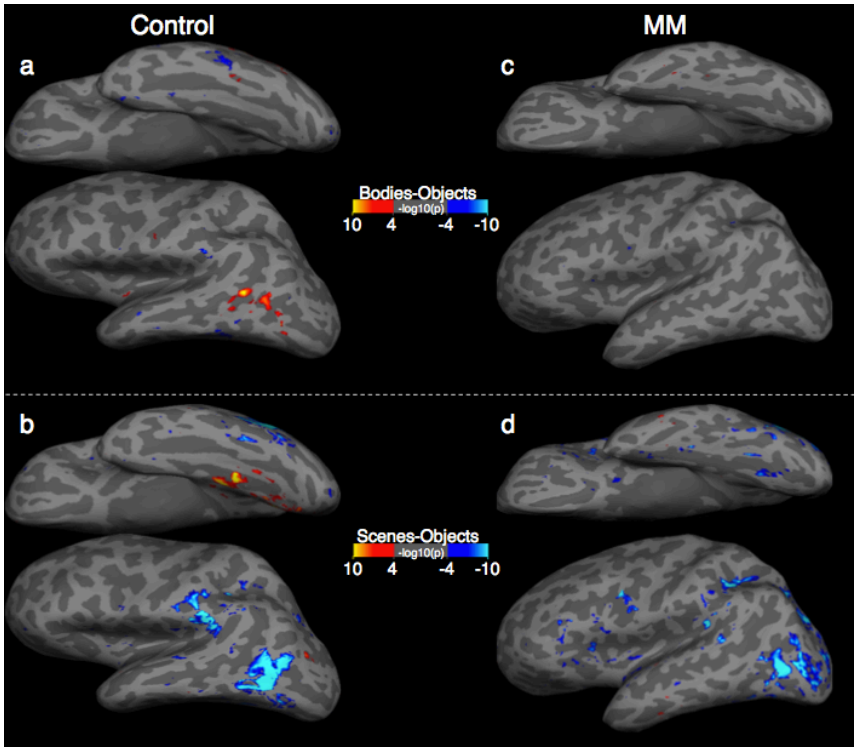

Figure 3.7. Ventral and lateral views of inflated left hemispheres showing results of the contrasts between bodies and objects (a, c) and scenes and objects (b, d). Results are shown separately for 1 control subject (left column) and for M. M. (right column). Data were averaged across four scans (in which stimuli were blurred and monocularly viewed) for the control subject and eight scans for M. M. Results are displayed at a threshold of $|p| < .0001$.

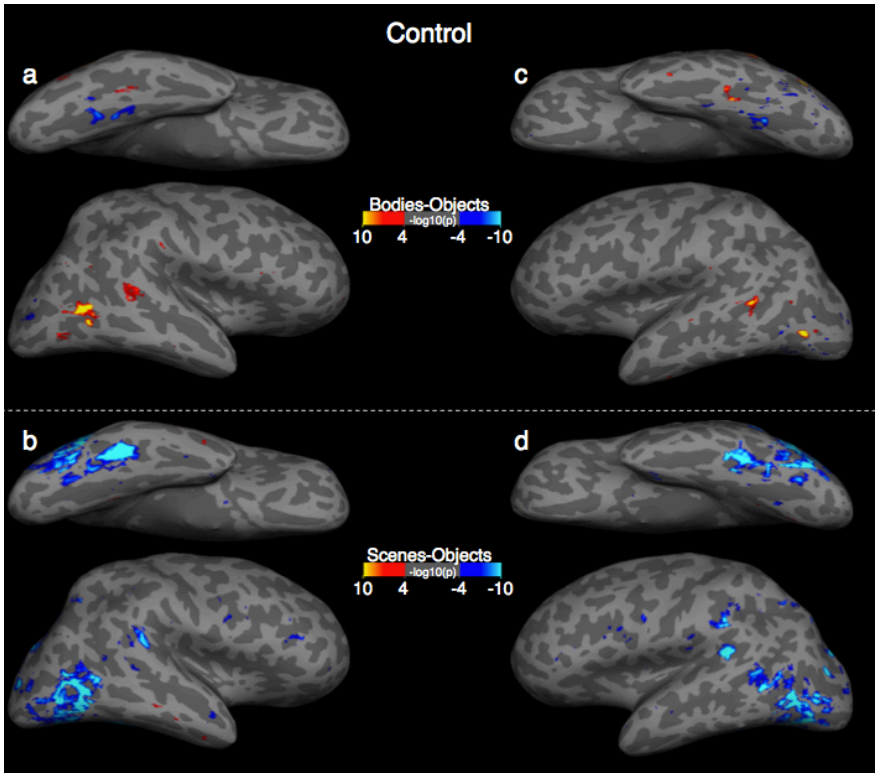

Figure 3.8. Ventral and lateral views of inflated cortical hemispheres showing results of the contrasts between bodies and objects (a, c) and scenes and objects (b, d) for the second control subject. Data were averaged across four scans (in which stimuli were blurred and monocularly viewed). Results are displayed at a threshold of $|p| < .0001$.

Body selectivity.

Control subjects showed the expected pattern of body-selective responses in the lateral occipital and ventral temporal cortex (Fig. 3.6a) in both hemispheres (Fig 3.7A). While we saw little evidence of the typical ventral temporal responses to bodies at a conventional threshold in M.M., we did observe body-selective responses in a region consistent with the extrastriate body area within the right hemisphere (Fig. 3.6c). There were no corresponding body-selective responses in the left hemisphere. With a very lenient threshold, we did observe a region in a location consistent with the fusiform body

area responding more strongly to bodies than to objects, though these responses were again not clearly differentiable from noise.

DISCUSSION

Visual function continues to develop throughout childhood and into early adolescence, with performance on tasks such as object recognition and face processing reaching adult like levels between the ages of 5 to 8 and 4 to 6 years, respectively, while remaining sensitive to deprivation for several years afterward (McKone et al., 2012; Nishimura et al., 2009). Subject M.M.'s vision developed normally up to 3.5 years of age, after which he experienced an extended period of visual deprivation until his sight was restored well after adolescence. As such, his case provides a unique opportunity to assess both the limits of plasticity in later adulthood and the influence of early vision on recovery from long-term blindness.

Tests carried out with M.M. shortly after surgery suggested that he had normal perception of color and motion, and only modest deficits in perception of simple form. M.M. shows essentially normal cortical responses to visual-motion stimuli (Fine et al., 2003), consistent with his behavioral sensitivity to motion cues, though these responses seem to coexist with auditory-motion responses not present in sighted individuals (Saenz, Lewis, Huth, Fine, & Koch, 2008). Consistent with M.M.'s ability to interpret simple 2-D forms, described first by Fine et al. (2003) and examined further here, our present results show relatively normal responses in the cortical region known as LOC, which has been implicated in the processing of object shape (Grill-Spector et al., 1999). One possibility is

that spared perception of color, motion, and shape reflects hard wiring of these faculties; indeed, evidence suggests that this may be the case with basic color processing (Mancuso et al., 2009). Alternatively, preservation of these faculties may indicate that their periods of sensitivity to deprivation end prior to 3.5 years of age.

Several recent studies have suggested that cross-modal responses resulting from early blindness may follow an organization that is analogous to that of at least some high-level visual areas in normally sighted individuals. For instance, cortical regions typically associated with visual object processing have been implicated in object-size estimation in the congenitally blind (Mahon, Anzellotti, Schwarzbach, Zampini, & Caramazza, 2009), and these regions contain information about similarities in object shape in both sighted and blind participants (Peelen, He, Han, Caramazza, & Bi, 2014). Activity has also been reported in the visual word form area during Braille reading (Buchel, Price, & Friston, 1998; Reich, Szwed, Cohen, & Amedi, 2011), and the emergence of body-selective regions in congenitally blind subjects has been reported as a result of training with soundscapes representing bodies (Striem-Amit & Amedi, 2014). Similarly, activation of common regions during visual and haptic recognition of facial expressions in sighted and blind subjects (Kitada et al., 2013) suggests that haptic experience may be sufficient for development of these regions in the absence of visual input.

Although M.M. had normal sight until 3.5 years of age, the literature suggests that this is well within the period when some forms of cross-modal plasticity occur (e.g., Burton et al., 2002; Gougoux et al., 2009; Sadato, Okada, Honda, & Yonekura, 2002), and he shows robust cross-modal responses to auditory-motion stimuli (Saenz et al., 2008). However, beyond the auditory-motion responses in hMT+, we do not know the

extent of cortical cross-modal responses in M.M. Further, it is unclear whether any existing cross-modal responses would facilitate or interfere with restored visual function. As described previously, M.M. has essentially normal perception of visual motion, and his responses to both visual and auditory motion within hMT+ are robust. In contrast, despite several years of early visual experience and more than a decade of recovered sight, M.M. remains profoundly impaired at interpreting visual facial expressions, which suggests that his haptic experience with faces and voice perception (Gougoux et al., 2009) did not lead to the preservation of neural architecture relevant for visual face recognition. Similarly, although we did observe relatively normal selectivity for bodies and objects within LOC, we found little to no evidence of high-level visual responses in ventral temporal cortex selective for face, body, scene, or object stimuli in M.M.

Shortly after recovering his sight, M.M. showed severe behavioral deficits in high-level visual tasks, and our follow-up tests revealed these to be long-standing impairments. When asked what challenges to vision remained in his daily life, M.M. replied "I have learned what works with vision and what doesn't, so I really don't challenge my vision much anymore." M.M. now uses a combination of vision and other modalities for specific tasks. "This means where motion or color might be clues, I use my vision. Where details might be required, like reading print or recognizing who someone is, I use tactile and auditory techniques."

In conclusion, M.M. continues to show severe behavioral impairments in 3-D form, object, and face processing with no evidence of improvement of recognition performance even after more than a decade of recovered vision. These behavioral impairments are associated with highly attenuated category-selective activity in ventral

visual cortex, which suggests that adult high-level vision is based on a visual architecture that is still sensitive to deprivation at the age of 3 years, and which has only limited plasticity in adulthood.

FINAL REMARKS

The studies described in this dissertation suggest that longstanding blindness alters the cortical representation of auditory frequency, leading to narrower tuning within auditory cortex (Chapter 1), and novel representations within occipital cortex (Chapter 2). Moreover, sight-recovery subjects show tuning to auditory frequency alongside cortical visual motion responses, suggesting stability in the cross-modal reorganization that occurs during blindness. This coincides with stability in the visual processing deficits observed in one of these individuals.

Our model of frequency tuning allows us to quantify these effects, and facilitates comparison with behavioral measures. Future work should extend this model to test hypotheses about functional reorganization in the human brain, perhaps modeling more complex feature spaces based on predictions from models of cortical organization and/or behavioral effects.

REFERENCES

Amedi A, Raz N, Pianka P, Malach R, Zohary E (2003). Early "visual" cortex activation correlates with superior verbal memory performance in the blind. Nat Neurosci, 6(7):758–766.

Amitay S, Hawkey DJ, Moore DR (2005) Auditory frequency discrimination learning is affected by stimulus variability. Percept Psychophys 67:691-698.

Bavelier, D., Levi, D. M., Li, R. W., Dan, Y., & Hensch, T. K. (2010). Removing brakes on adult brain plasticity: From molecular to behavioral interventions. Journal of Neuroscience, 30, 14964–14971. doi:10.1523/JNEUROSCI.4812-10.2010

Bedny, M., Konkle, T., Pelphrey, K., Saxe, R., and Pascual-Leone, A. (2010). Sensitive period for a multimodal response in human visual motion area MT/MST. Curr. Biol. 20, 1900–1906. doi: 10.1016/j.cub.2010.09.044

Bedny, M., Pascual-Leone, A., Dodell-Feder, D., Fedorenko, E., and Saxe, R. (2011). Language processing in the occipital cortex of congenitally blind adults. Proc. Natl. Acad. Sci. U S A 108, 4429–4434. doi: 10.1073/pnas.10148 18108

Bock, A. S., Saenz, M., Tungaraza, R., Boynton, G. M., Bridge, H., and Fine, I. (2013). Visual callosal topography in the absence of retinal input. Neuroimage 81, 325–334. doi: 10.1016/j.neuroimage.2013.05.038

Born RT, Bradley DC (2005). Structure and function of visual area MT. Annu Rev Neurosci. 2005;28:157-89.

Boynton GM, Engel SA, Glover GH, Heeger DJ (1996) Linear systems analysis of functional magnetic resonance imaging in human V1. The Journal of Neuroscience 16:4207-4221.

Boynton GM, Demb JB, Glover GH, Heeger DJ (1999) Neuronal basis of contrast discrimination. Vision research 39:257-269.

Buracas GT, Fine I, Boynton GM (2005) The relationship between task performance and functional magnetic resonance imaging response. The Journal of neuroscience : the official journal of the Society for Neuroscience 25:3023-3031.

Buchel, C., Price, C., & Friston, K. (1998). A multimodal language region in the ventral visual pathway. Nature, 394, 274–277. doi:10.1038/28389

Burton, H., Snyder, A. Z., Conturo, T. E., Akbudak, E., Ollinger, J. M., & Raichle, M. E. (2002). Adaptive changes in early and late blind: A fMRI study of Braille reading. Journal of Neurophysiology, 87, 589–607.

Bregman AS1, Liao C, Levitan R. (1990). Auditory grouping based on fundamental frequency and formant peak frequency. Can J Psychol., 44(3):400-13.

Bridge, H., Cowey, A., Ragge, N., and Watkins, K. (2009). Imaging studies in congenital anophthalmia reveal preservation of brain architecture in 'visual' cortex. Brain 132, 3467–3480. doi: 10.1093/brain/awp279

Cheselden, W. (1753). An account of some observations made by a young gentleman, who was born blind, or lost his sight so early, that he had no remembrance of ever having seen, and was couch'd between 13 and 14 years of age. Philosophical Transactions, 35, 447–450. doi:10.2307/103697

Cohen et al. (1997). Functional relevance of cross-modal plasticity in blind humans. *Nature*, 389:180–183

Collignon O, Dormal G, Albouy G, Vandewalle G, Voss P, Phillips C, Lepore F (2013) Impact of blindness onset on the functional organization and the connectivity of the occipital cortex. Brain 136:2769-2783.

Collignon, O., Vandewalle, G., Voss, P., Albouy, G., Charbonneau, G., Lassonde, M., et al. (2011). Functional specialization for auditory-spatial processing in the occipital cortex of congenitally blind humans. Proc. Natl. Acad. Sci. U S A 108, 4435–4440. doi: 10.1073/pnas.1013928108

Cox, R. W., & Jesmanowicz, A. (1999). Real-time 3D image registration for functional MRI. Magnetic Resonance in Medicine, 42, 1014–1018.

Da Costa S, van der Zwaag W, Marques JP, Frackowiak RS, Clarke S, Saenz M (2011) Human primary auditory cortex follows the shape of Heschl's gyrus. J Neurosci 31:14067-14075.

Da Costa S, van der Zwaag W, Miller LM, Clarke S, Saenz M (2013) Tuning in to sound: frequency-selective attentional filter in human primary auditory cortex. J Neurosci 33:1858-1863.

De Volder, A. G., Bol, A., Blin, J., Robert, A., Arno, P., Grandin, C., et al. (1997). Brain energy metabolism in early blind subjects: neural activity in the visual cortex. Brain Res. 750, 235–244. doi: 10.1016/s0006-8993(96) 01352-2

Dick F, Tierney AT, Lutti A, Josephs O, Sereno MI, Weiskopf N (2012) In vivo functional and myeloarchitectonic mapping of human primary auditory areas. The Journal of neuroscience : the official journal of the Society for Neuroscience 32:16095-16105.

Dormal G, Lepore F, Harissi-Dagher M, Albouy G, Bertone A, Rossion B, Collignon O. (2014). Tracking the evolution of crossmodal plasticity and visual functions before and after sight restoration. J Neurophysiology, 113(6):1727-42. doi: 10.1152/jn.00420.2014.

Downing, P. E., Jiang, Y., Shuman, M., & Kanwisher, N. (2001). A cortical area selective for visual processing of the human body. Science, 293, 2470–2473. doi:10.1126/science.1063414

Dumoulin SO, Wandell BA (2008) Population receptive field estimates in human visual cortex. Neuroimage 39:647-660.

Duncan RO, Boynton GM (2003) Cortical magnification within human primary visual cortex correlates with acuity thresholds. Neuron 38:659-671.

Elbert T, Sterr A, Rockstroh B, Pantev C, Muller MM, Taub E (2002) Expansion of the tonotopic area in the auditory cortex of the blind. J Neurosci 22:9941-9944.

Ellemberg, D., Lewis, T. L., Defina, N., Maurer, D., Brent, H. P., Guillemot, J. P., & Lepore, F. (2005). Greater losses in sensitivity to second-order local motion than to first-order local motion after early visual deprivation in humans. Vision Research, 45, 2877–2884. doi:10.1016/j.visres.2004.11.019

Epstein, R., & Kanwisher, N. (1998). A cortical representation of the local visual environment. Nature, 392, 598–601. doi:10.1038/33402.

Fine, I., Wade, A. R., Brewer, A. A., May, M. G., Goodman, D. F., Boynton, G. M., . . . MacLeod, D. I. A. (2003). Long-term deprivation affects visual perception and cortex. Nature Neuroscience, 6, 915–916. doi:10.1038/nn1102

Formisano E, Kim DS, Di Salle F, van de Moortele PF, Ugurbil K, Goebel R (2003) Mirror- symmetric tonotopic maps in human primary auditory cortex. Neuron 40:859-869.
Goel A, Jiang B, Xu LW, Song L, Kirkwood A, Lee HK (2006) Cross-modal regulation of synaptic AMPA receptors in primary sensory cortices by visual experience. Nat Neurosci 9:1001-1003.
Golubic SJ, Susac A, Grilj V, Ranken D, Huonker R, Haueisen J, Supek S (2011) Size matters: MEG empirical and simulation study on source localization of the earliest visual activity in the occipital cortex. Medical & biological engineering & computing 49:545-554.
Gori, M., Sandini, G., Martinoli, C., and Burr, D. C. (2014). Impairment of auditory spatial localization in congenitally blind human subjects. Brain 137, 288–293. doi: 10.1093/brain/awt311
Gougoux F, Zatorre RJ, Lassonde M, Voss P, Lepore F. (2005). A functional neuroimaging study of sound localization: visual cortex activity predicts performance in early-blind individuals. *PLoS Biol*, 3(2):27.
Gougoux F, Lepore F, Lassonde M, Voss P, Zatorre RJ, Belin P (2004) Neuropsychology: pitch discrimination in the early blind. Nature 430:309.
Gougoux, F., Belin, P., Voss, P., Lepore, F., Lassonde, M., & Zatorre, R. J. (2009). Voice perception in blind persons: A functional magnetic resonance imaging study. Neuropsychologia, 47, 2967–2974. doi:10.1016/j.neuropsychologia.2009.06.027
Grantham, D. W. Auditory Motion Aftereffects in the Horizontal Plane: The Effects of Spectral Region, Spatial Sector, and Spatial Richness. Acta Acustica, 84(2):337-347
Gregory, R. L., & Wallace, J. G. (1963). Recovery from early blindness: A case study. Retrieved from http://www.richardgregory.org/papers/recovery_blind/recovery-from-early-blindness.pdf
Greve, D. N., & Fischl, B. (2009). Accurate and robust brain image alignment using boundary-based registration. NeuroImage, 48, 63–72. doi:10.1016/j.neuroimage.2009.06.060
Grill-Spector, K., Kushnir, T., Edelman, S., Avidan, G., Itzchak, Y., & Malach, R. (1999). Differential processing of objects under various viewing conditions in the human lateral occipital complex. Neuron, 24, 187–203.
Hackett TA (2008) Anatomical organization of the auditory cortex. Journal of the American Academy of Audiology 19:774-779.
Hackett TA, Stepniewska I, Kaas JH (1998) Subdivisions of auditory cortex and ipsilateral cortical connections of the parabelt auditory cortex in macaque monkeys. The Journal of comparative neurology 394:475-495.
Humphries C, Liebenthal E, Binder JR (2010) Tonotopic organization of human auditory cortex. Neuroimage 50:1202-1211.
Jäncke L, Gaab N, Wüstenberg T, Scheich H, Heinze HJ (2001) Short-term functional plasticity in the human auditory cortex: an fMRI study. Cognitive Brain Research 12:479-485.
Jiang F, Stecker GC, Fine I (2014) Auditory motion processing after early blindness. J Vis 14:4.

Julian, J. B., Fedorenko, E., Webster, J., & Kanwisher, N. (2012). An algorithmic method for functionally defining regions of interest in the ventral visual pathway. NeuroImage, 60, 2357–2364. doi:10.1016/j.neuroimage.2012.02.055

Kalia, A., Lesmes, L. A., Dorr, M., Gandhi, T., Chatterjee, G., Ganesh, S., . . . Sinha, P. (2014). Development of pattern vision following early and extended blindness. Proceedings of the National Academy of Sciences, USA, 111, 2035–2039. doi:10.1073/pnas.1311041111

Kanwisher, N., & Dilks, D. D. (2013). The functional organization of the ventral visual pathway in humans. In J. S. Werner & L. M. Chalupa (Eds.), The new visual neurosciences (pp. 733–748). Cambridge, MA: MIT Press.

Kanwisher, N., McDermott, J., & Chun, M. M. (1997). The fusiform face area: A module in human extrastriate cortex specialized for face perception. Journal of Neuroscience, 17, 4302–4311.

Karlen, S. J., and Krubitzer, L. (2009). Effects of bilateral enucleation on the size of visual and nonvisual areas of the brain. Cereb. Cortex 19, 1360–1371. doi: 10. 1093/cercor/bhn176

Kayser C, Petkov CI, Logothetis NK (2007a) Tuning to Sound Frequency in Auditory Field Potentials. Journal of neurophysiology 98:1806-1809.

Kayser C, Petkov CI, Augath M, Logothetis NK (2007b) Functional imaging reveals visual modulation of specific fields in auditory cortex. The Journal of neuroscience : the official journal of the Society for Neuroscience 27:1824-1835.

Kitada, R., Okamoto, Y., Sasaki, A. T., Kochiyama, T., Miyahara, M., Lederman, S. J., & Sadato, N. (2013). Early visual experience and the recognition of basic facial expressions: Involvement of the middle temporal and inferior frontal gyri during haptic identification by the early blind. Frontiers in Human Neuroscience, 7, Article 7. Retrieved from http://journal.frontiersin.org/Journal/10.3389/fnhum.2013.00007/full

Kourtzi, Z., & Kanwisher, N. (2001). Representation of perceived object shape by the human lateral occipital complex. Science, 293, 1506–1509. doi:10.1126/science.1061133

Kujala T, Alho K, Paavilainen P, Summala H, Naatanen R (1992) Neural plasticity in processing of sound location by the early blind: an event-related potential study. Electroencephalogr Clin Neurophysiol 84:469-472.

Kujala T, Huotilainen M, Sinkkonen J, Ahonen AI, Alho K, Hamalainen MS, Ilmoniemi RJ, Kajola M, Knuutila JE, Lavikainen J, et al. (1995) Visual cortex activation in blind humans during sound discrimination. Neurosci Lett 183:143-146.

Kupers, R., and Ptito, M. (2014). Compensatory plasticity and cross-modal reorganization following early visual deprivation. Neurosci. Biobehav. Rev. 41, 36–52. doi: 10.1016/j.neubiorev.2013.08.001

Langers DRM, van Dijk P (2011) Mapping the Tonotopic Organization in Human Auditory Cortex with Minimally Salient Acoustic Stimulation. Cerebral Cortex.

Langers DRM, Krumbholz K, Bowtell RW, Hall DA (2014a) Neuroimaging paradigms for tonotopic mapping (I): The influence of sound stimulus type. NeuroImage 100:650-662.

Lee HK, Whitt JL (2015) Cross-modal synaptic plasticity in adult primary sensory cortices. Curr Opin Neurobiol 35:119-126.

Le Grand, R., Mondloch, C. J., Maurer, D., & Brent, H. P. (2004). Impairment in holistic face processing following early visual deprivation. Psychological Science, 15, 762–768. doi:10.1111/j.0956-7976.2004.00753.

Lessard N, Pare M, Lepore F, Lassonde M (1998) Early-blind human subjects localize sound sources better than sighted subjects. Nature 395:278-280.

Levin, N., Dumoulin, S. O., Winawer, J., Dougherty, R. F., & Wandell, B. A. (2010). Cortical maps and white matter tracts following long period of visual deprivation and retinal image restoration. Neuron, 65, 21–31. doi:10.1016/j.neuron.2009.12.006

Lewis, T. L., Ellemberg, D., Maurer, D., Wilkinson, F., Wilson, H. R., Dirks, M., & Brent, H. P. (2002). Sensitivity to global form in glass patterns after early visual deprivation in humans. Vision Research, 42, 939–948.

Lewis, T. L., & Maurer, D. (2005). Multiple sensitive periods in human visual development: Evidence from visually deprived children. Developmental Psychobiology, 46, 163–183. doi:10.1002/dev.20055

Mahon, B. Z., Anzellotti, S., Schwarzbach, J., Zampini, M., & Caramazza, A. (2009). Category-specific organization in the human brain does not require visual experience. Neuron, 63, 397–405. doi:10.1016/j.neuron.2009.07.012

Malach, R., Reppas, J. B., Benson, R. R., Kwong, K. K., Jiang, H., Kennedy, W. A., . . . Tootell, R. B. (1995). Object-related activity revealed by functional magnetic resonance imaging in human occipital cortex. Proceedings of the National Academy of Sciences, USA, 92, 8135–8139.

Mancuso, K., Hauswirth, W. W., Li, Q., Connor, T. B., Kuchenbecker, J. A., Mauck, M. C., . . . Neitz, M. (2009). Gene therapy for red-green colour blindness in adult primates. Nature, 461, 784–787. doi:10.1038/nature08401

Maurer, D., Mondloch, C. J., & Lewis, T. L. (2007). Effects of early visual deprivation on perceptual and cognitive development. Progress in Brain Research, 164, 87–104. doi:10.1016/S0079-6123(07)64005-9

McKone, E., Crookes, K., Jeffery, L., & Dilks, D. D. (2012). A critical review of the development of face recognition: Experience is less important than previously believed. Cognitive Neuropsychology, 29, 174–212. doi:10.1080/02643294.2012.660138

Moerel M, De Martino F, Formisano E (2012) Processing of Natural Sounds in Human Auditory Cortex: Tonotopy, Spectral Tuning, and Relation to Voice Sensitivity. The Journal of Neuroscience 32:14205-14216.

Moerel M, De Martino F, Formisano E (2014) An anatomical and functional topography of human auditory cortical areas. Frontiers in Neuroscience 8.

Movshon, J. A., and Van Sluyters, R. C. (1981). Visual neural development. Annu. Rev. Psychol. 32, 477–522. doi: 10.1146/annurev.ps.32.020181. 002401

Nishimura, M., Scherf, S., & Behrmann, M. (2009). Development of object recognition in humans. F1000 Biology Reports, 1, 56. doi:10.3410/B1-56

Ostrovsky, Y., Andalman, A., & Sinha, P. (2006). Vision following extended congenital blindness. Psychological Science, 17, 1009–1014. doi:10.1111/j.1467-9280.2006.01827.x

Ostrovsky, Y., Meyers, E., Ganesh, S., Mathur, U., & Sinha, P. (2009). Visual parsing after recovery from blindness. Psychological Science, 20, 1484–1491. doi:10.1111/j.1467-9280.2009.02471.

Pascual-Leone, A., Amedi, A., Fregni, F., and Merabet, L. B. (2005). The plastic human brain cortex. Annu. Rev. Neurosci. 28, 377–401. doi: 10.1146/annurev. neuro.27.070203.144216

Pascual-Leone, A., and Hamilton, R. (2001). The metamodal organization of the brain, in Progress in Brain Research, eds C. Casanova and M. Ptito (San Diego CA: Elsevier Science), 1–19.

Pascual-Leone A, Torres F (1993) Plasticity of the sensorimotor cortex representation of the reading finger in Braille readers. Brain 116 (Pt 1):39-52.

Peelen, M. V., He, C., Han, Z., Caramazza, A., & Bi, Y. (2014). Nonvisual and visual object shape representations in occipitotemporal cortex: Evidence from congenitally blind and sighted adults. Journal of Neuroscience, 34, 163–170. doi:10.1523/JNEUROSCI.1114-13.2014

Petkov CI, Kayser C, Augath M, Logothetis NK (2006) Functional imaging reveals numerous fields in the monkey auditory cortex. PLoS biology 4:e215.

Petrus E, Isaiah A, Jones AP, Li D, Wang H, Lee HK, Kanold PO (2014) Crossmodal induction of thalamocortical potentiation leads to enhanced information processing in the auditory cortex. Neuron 81:664-673.

Petrus E, Rodriguez G, Patterson R, Connor B, Kanold PO, Lee HK (2015) Vision loss shifts the balance of feedforward and intracortical circuits in opposite directions in mouse primary auditory and visual cortices. J Neurosci 35:8790-8801.

Rademacher J, Morosan P, Schormann T, Schleicher A, Werner C, Freund HJ, Zilles K (2001) Probabilistic mapping and volume measurement of human primary auditory cortex. Neuroimage 13:669-683.

Rajimehr, R., Devaney, K. J., Bilenko, N. Y., Young, J. C., & Tootell, R. B. (2011). The "parahippocampal place area" responds preferentially to high spatial frequencies in humans and monkeys. PLoS Biology, 9(4), Article e1000608. doi:10.1371/journal.pbio.1000608

Rauschecker JP (1995) Compensatory plasticity and sensory substitution in the cerebral cortex. Trends Neurosci 18:36-43.

Recanzone GH, Schreiner CE, Merzenich MM (1993) Plasticity in the frequency representation of primary auditory cortex following discrimination training in adult owl monkeys. J Neurosci 1993 Jan;13(1 87-103): 13:87-103.

Renier, L., De Volder, A. G., and Rauschecker, J. P. (2014). Cortical plasticity and preserved function in early blindness. Neurosci. Biobehav. Rev. 41, 53–63. doi: 10. 1016/j.neubiorev.2013.01.025

Renier L, Cuevas I, Grandin CB, Dricot L, Plaza P, Lerens E, Rombaux P, De Volder AG. (2013). Right occipital cortex activation correlates with superior odor processing performance in the early blind. PLoS One, 8(8):e71907. doi: 10.1371/

Reich, L., Szwed, M., Cohen, L., & Amedi, A. (2011). A ventral visual stream reading center independent of visual experience. Current Biology, 21, 363–368. doi:10.1016/j.cub.2011.01.040

Robbins, R. A., Nishimura, M., Mondloch, C. J., Lewis, T. L., & Maurer, D. (2010). Deficits in sensitivity to spacing after early visual deprivation in humans: A

comparison of human faces, monkey faces, and houses. Developmental Psychobiology, 52, 775–781. doi:10.1002/dev.20473
Röder, B., Rösler, F., and Neville, H. J. (2001). Auditory memory in congenitally blind adults: a behavioral-electrophysiological investigation. Brain Res. Cogn. Brain Res. 11, 289–303. doi: 10.1016/s0926-6410(01)00002-7
Röder, B., Teder-Sälejärvi, W., Sterr, A., Rösler, F., Hillyard, S. A., and Neville, H. J. (1999). Improved auditory spatial tuning in blind humans. Nature 400, 162– 166. doi: 10.1038/22106
Sadato, N., Okada, T., Honda, M., & Yonekura, Y. (2002). Critical period for cross-modal plasticity in blind humans: A functional MRI study. NeuroImage, 16, 389–400.
Saenz M, Langers DR (2014) Tonotopic mapping of human auditory cortex. Hear Res 307:42-52.
Saenz, M., Lewis, L. B., Huth, A. G., Fine, I., & Koch, C. (2008). Visual motion area MT+/V5 responds to auditory motion in human sight-recovery subjects. Journal of Neuroscience, 28, 5141–5148. doi:10.1523/JNEUROSCI.0803-08.2008
Scharff, A., Palmer, J., & Moore, C. M. (2013). Divided attention limits perception of 3-D object shapes. Journal of Vision, 13(2), Article 18. Retrieved from http://www.journalofvision.org/content/13/2/18.full
Šikl, R., Šimeček, M., Porubanová-Norquist, M., Bezdíček, O., Kremláček, J., Stodůlka, P., . . . Ostrovsky, Y. (2013). Vision after 53 years of blindness. i-Perception, 4, 498–507.
Sinha, P., & Held, R. (2012). Sight restoration. F1000 Medicine Reports, 4, 17. doi:10.3410/M4-17
Smith, S. M. (2002). Fast robust automated brain extraction. Human Brain Mapping, 17, 143–155. doi:10.1002/hbm.10062
Spearman C (1904) The proof and measurement of association between two things. The American journal of psychology 15:72-101.
Starlinger I, Niemeyer W. (1981) Do the blind hear better? Investigations on auditory processing in congenital or early acquired blindness. I. Peripheral functions. Audiology; 20(6):503-9.
Sterr A, Müller MM, Elbert T, Rockstroh B, Pantev C, Taub E. (1998). Perceptual correlates of changes in cortical representation of fingers in blind multifinger Braille readers. J Neurosci.18:4417–4423.
Stevens AA, Weaver KE (2009) Functional characteristics of auditory cortex in the blind. Behav Brain Res 196:134-138.
Stevens AA, Snodgrass M, Schwartz D, Weaver KE (2007). Preparatory Activity in Occipital Cortex in Early Blind Humans Predicts Auditory Perceptual Performance. The Journal of Neuroscience, 27(40):10734 –10741
Stevenson RE, Seaver LH, Collins JS, et al. (2004). Neural tube defects and associated anomalies in South Carolina.*Birth Defects Res A Clin Mol Teratol* **70**:554–558.
Striem-Amit E, Hertz U, Amedi A (2011) Extensive cochleotopic mapping of human auditory cortical fields obtained with phase-encoding FMRI. PLoS One 6:e17832.
Striem-Amit, E., & Amedi, A. (2014). Visual cortex extrastriate body-selective area activation in congenitally blind people "seeing" by using sounds. Current Biology, 24, 687–692. doi:10.1016/j.cub.2014.02.010

Talavage TM, Sereno MI, Melcher JR, Ledden PJ, Rosen BR, Dale AM (2004) Tonotopic Organization in Human Auditory Cortex Revealed by Progressions of Frequency Sensitivity. Journal of neurophysiology 91:1282-1296.

Thomas JM, Huber E, Stecker GC, Boynton GM, Saenz M, Fine I (2015) Population receptive field estimates of human auditory cortex. Neuroimage 105:428-439.

Valvo, A. (1971). Sight restoration after long-term blindness: The problems and behavior patterns of visual rehabilitation. New York, NY: American Foundation for the Blind.

Voss P, Zatorre RJ (2012) Occipital cortical thickness predicts performance on pitch and musical tasks in blind individuals. Cereb Cortex 22:2455-2465.

Voss P, Tabry V, Zatorre RJ (2015) Trade-off in the sound localization abilities of early blind individuals between the horizontal and vertical planes. J Neurosci 35:6051-6056.

Voss P, Lepore F, Gougoux F, Zatorre RJ (2011) Relevance of spectral cues for auditory spatial processing in the occipital cortex of the blind. Frontiers in psychology 2:48.

Wan CY, Wood AG, Reutens DC, Wilson SJ (2010) Early but not late-blindness leads to enhanced auditory perception. Neuropsychologia 48:344-348.

Watkins KE, Shakespeare TJ, O'Donoghue MC, Alexander I, Ragge N, Cowey A, Bridge H (2013) Early auditory processing in area V5/MT+ of the congenitally blind brain. J Neurosci 33:18242-18246.

Weaver, K. E., Richards, T. L., Saenz, M., Petropoulos, H., and Fine, I. (2013). Neurochemical changes within human early blind occipital cortex. Neuroscience 252, 222–233. doi: 10.1016/j.neuroscience.2013.08.004

Wiesel, T. N., and Hubel, D. H. (1963). Effects of visual deprivation on morphology and physiology of cells in the cats lateral geniculate body. J. Neurophysiol. 26, 978–993.

Wiesel, T. N., and Hubel, D. H. (1965a). Comparison of the effects of unilateral and bilateral eye closure on cortical unit responses in kittens. J. Neurophysiol. 28, 1029–1040.

Wiesel, T. N., and Hubel, D. H. (1965b). Extent of recovery from the effects of visual deprivation in kittens. J. Neurophysiol. 28, 1060–1072.

Wilcoxon, F. (1945). Individual Comparisons by Ranking Methods. Biometrics Bulletin, 1: 6, 80-83: http://links.jstor.org/sici?sici=0099-4987%28194512%291%3A6%3C80%3AICBRM%3E2.0.CO%3B2-P

Wohlgemuth, A. (1911). On the after-effect of seen movement. Cambridge, University Press.

Wolbers, T., Zahorik, P., and Giudice, N. A. (2011). Decoding the direction of auditory motion in blind humans. Neuroimage 56, 681–687. doi: 10.1016/j.neuroimage.2010.04.266